JCB

Article

SLAMF1 is required for TLR4-mediated TRAM-TRIF–dependent signaling in human macrophages

Maria Yurchenko,[1,3] Astrid Skjesol,[1] Liv Ryan,[1] Gabriel Mary Richard,[1] Richard Kumaran Kandasamy,[1] Ninghai Wang,[2] Cox Terhorst,[2] Harald Husebye,[1,3]* and Terje Espevik[1,3]*

[1]Centre of Molecular Inflammation Research, Norwegian University of Science and Technology, Trondheim, Norway
[2]Division of Immunology, Beth Israel Deaconess Medical Center, Harvard Medical School, Boston, MA
[3]The Central Norway Regional Health Authority, St. Olavs Hospital HF, Trondheim, Norway

Signaling lymphocytic activation molecule family 1 (SLAMF1) is an Ig-like receptor and a costimulatory molecule that initiates signal transduction networks in a variety of immune cells. In this study, we report that SLAMF1 is required for Toll-like receptor 4 (TLR4)-mediated induction of interferon β (IFNβ) and for killing of Gram-negative bacteria by human macrophages. We found that SLAMF1 controls trafficking of the Toll receptor–associated molecule (TRAM) from the endocytic recycling compartment (ERC) to *Escherichia coli* phagosomes. In resting macrophages, SLAMF1 is localized to ERC, but upon addition of *E. coli*, it is trafficked together with TRAM from ERC to *E. coli* phagosomes in a Rab11-dependent manner. We found that endogenous SLAMF1 protein interacted with TRAM and defined key interaction domains as amino acids 68 to 95 of TRAM as well as 15 C-terminal amino acids of SLAMF1. Interestingly, the SLAMF1–TRAM interaction was observed for human but not mouse proteins. Overall, our observations suggest that SLAMF1 is a new target for modulation of TLR4–TRAM–TRIF inflammatory signaling in human cells.

Introduction

Toll-like receptors (TLRs) are pivotal for the defense against multiple pathogens by recognizing pathogen-associated molecular patterns. TLR4 recognizes lipopolysaccharide (LPS) from Gram-negative bacteria in complex with the coreceptors myeloid differentiation factor 2 and CD14, and it recruits signaling adapters myeloid differentiation primary response gene 88 (MyD88) and MyD88 adapter–like (Mal). This results in an immediate activation of nuclear factor κB (NF-κB) and production of proinflammatory cytokines. TLR4 is also present on endosomes and phagosomes to which the signaling adapter Toll receptor–associated molecule (TRAM) is recruited (Husebye et al., 2006, 2010; Kagan et al., 2008). The mechanism controlling TRAM recruitment remains unclear but seems to be Rab11 dependent (Husebye et al., 2010; Klein et al., 2015).

TRAM is crucial for the subsequent recruitment of Toll/interleukin (IL)-1 receptor (TIR) domain–containing adapter-inducing IFN-β (TRIF) and other downstream molecules, leading to IFNβ secretion (Fitzgerald et al., 2003b; Oshiumi et al., 2003; Yamamoto et al., 2003; Husebye et al., 2010). The role of endogenous type I IFNs in host defense against bacterial infections could be either beneficial or detrimental. Type I IFNs make macrophages more sensitive to cell death–inducing stimuli that could favor bacterial replication and release (Trinchieri, 2010). At the same time, type I IFNs are required for the host resistance to group B streptococci, pneumococci, and *Escherichia coli* (Mancuso et al., 2007).

Assembly of the TLR4–TRAM–TRIF complex followed by the activation of TANK-binding kinase 1 (TBK1) results not only in the induction of type I IFNs but also is required for maintenance of the integrity of pathogen-containing vacuoles and restriction of bacterial proliferation in the cytosol (Radtke et al., 2007; Thurston et al., 2016). Moreover, TBK1 activates the Akt–mTOR–HIF1α signaling axis, which orchestrates metabolic reprogramming to aerobic glycolysis in immune cells (Krawczyk et al., 2010; Everts et al., 2014). Glycolysis provides ATP for driving phagocytosis, proinflammatory cytokine production, and NADPH for the NADPH oxidase 2 (NOX2) enzyme to generate reactive oxygen species (ROS; Kelly and O'Neill, 2015).

Signaling lymphocytic activation molecule family 1 (SLAMF1)/CD150 is a type I glycoprotein belonging to the SLAM subfamily of the CD2-like family of proteins (Sidorenko and Clark, 1993; Cocks et al., 1995). SLAMF1 acts as a coreceptor that can modulate signaling via the TNF family and antigen receptors (Mikhalap et al., 1999; Wang et al., 2004; Réthi et al., 2006; Makani et al., 2008). SLAMF1 is involved in the regulation of innate immune responses. *Slamf1*$^{-/-}$ bone marrow–derived macrophages (BMDMs) are deficient in bacterial killing as they produce less ROS in response to *Escherichia coli*. Mouse SLAMF1 positively regulates NOX2 activity by forming a complex with beclin-1–Vps34–Vps15–UVRAG

*H. Husebye and T. Espevik contributed equally to this paper.

Correspondence to Maria Yurchenko: mariia.yurchenko@ntnu.no

The Rockefeller University Press
J. Cell Biol. Vol. 217 No. 4 1411–1429
https://doi.org/10.1083/jcb.201707027

(Berger et al., 2010; Ma et al., 2012). Thus, it was essential to explore the contribution of SLAMF1 to TLR4-mediated signaling in human cells. In this study, we show that in human macrophages, SLAMF1 acts as a critical regulator of TLR4-mediated signaling from the phagosome by interacting with TRAM adapters and class I Rab11 family interacting proteins (FIPs) and recruiting the adapter to the TLR4 signaling complex.

Results

SLAMF1 is expressed in human macrophages and localized to the Rab11-positive endocytic recycling compartment (ERC)

Previous studies have suggested that SLAMF1 is found in intracellular compartments of human primary dendritic cells and glioblastoma cells (Avota et al., 2011; Romanets-Korbut et al., 2015). Human peripheral blood monocytes do not express SLAMF1 on the plasma membrane (Farina et al., 2004; Romero et al., 2004). Therefore, we first analyzed the cellular distribution of SLAMF1 in human monocytes, macrophages, and THP-1 cells by confocal microscopy. In all the cell types examined, the major pool of SLAMF1 was located in a perinuclear area negative for the Golgi marker GM130 (Fig. 1, A and B). To further define SLAMF1 localization, monocytes were costained with markers for different types of endosomes: recycling (Rab11a; Fig. 1 C), early (EEA1), and late endosomes (LAMP1; Fig. 1, D and E). Rab11a also defines the ERC, a condensed perinuclear region containing tubular membrane structures that originate from the microtubule organizing center (Yamashiro et al., 1984). TRAM and TLR4 are also present in ERCs of human monocytes and macrophages (Husebye et al., 2010; Klein et al., 2015).

A marked colocalization was found between SLAMF1 and Rab11 in ERCs of resting cells with a Manders's colocalization coefficient of tM = 0.683 ± 0.08 (Fig. 1 C), whereas there was no colocalization with the other endosomal markers (Fig. 1, D and E). As determined by flow cytometry, only 1% of the monocytes and 4% of macrophages showed surface expression of SLAMF1, whereas 40% of the differentiated THP-1 cells were SLAMF1 positive (Fig. 1 F). LPS stimulation increased the surface expression of SLAMF1 in primary macrophages by >50% after 6 h of LPS stimulation, with an increase in the total SLAMF1 protein expression (Fig. 1, G and H; and Fig. S1 A). Moreover, various TLR ligands such as Pam3Cys (TLR1/2), FSL-1 (TLR2/6), R848 (TLR7 and -8), and CL075 (TLR8) increased *SLAMF1* mRNA expression in monocytes and macrophages (Fig. 1, I and J), with *E. coli* being the most potent stimulator (Fig. 1 I). These results indicate that several TLRs control SLAMF1 expression in human cells.

In summary, resting macrophages showed very low SLAMF1 surface level expression, and the major cellular pool of SLAMF1 was found to be in the ERC. THP-1 cells had more surface SLAMF1, but the major cellular pool was still located in the ERC. These observations suggest that ERC-located SLAMF1 may have a yet-undefined function in macrophages.

SLAMF1 is required for TLR4-mediated IFNβ production, but its expression is not regulated by the IFNα/β receptor (IFNAR)

Next, we used siRNAs to target SLAMF1 in THP-1 cells (Fig. 2 A) and human macrophages (Fig. 2 B). We found that SLAMF1 silencing caused consistent reduction in LPS-mediated *IFNβ* mRNA levels (Fig. 2, A and B) and IFNβ secretion (Fig. 2, C and D). In contrast, *TNF* mRNA amounts were only reduced at late time points of LPS stimulation, and secretion was affected only in THP-1 cells (Fig. 2, A–D). SLAMF1 silencing impaired both IL-6 and CXCL10 secretion but did not affect the secretion of IL-1β and IL-8 in THP-1 cells and human macrophages (Fig. 2, E and F). The phosphorylation of STAT1 and the initiation of transcription of IFN-inducible genes like *CXCL10* are readouts of IFNβ binding to the IFNAR (Toshchakov et al., 2002). IFNAR-dependent STAT1 phosphorylation (Y701) and *CXCL10* mRNA expression in response to LPS were both significantly decreased in THP-1 cells pretreated by anti-IFNAR α/β chain 2 mAbs (Fig. S1, B and C). However, *SLAMF1* mRNA expression was not altered by blocking IFNAR (Fig. S1 D). Thus, *SLAMF1* mRNA expression was not driven by IFNβ-mediated signaling.

Upon stimulation with *E. coli* particles, *SLAMF1*-silenced THP-1 cells also showed a consistent reduction in *IFNβ* and *TNF* mRNA (Fig. S2 A). However, SLAMF1 silencing in macrophages had no effect on *IFNβ* or *TNF* mRNA expression in response to polyinosinic-polycytidylic acid (poly I:C) with or without transfection (RIG-I/MDA5 or TLR3) or to the TLR8 ligand CL075 (Fig. S2, B–D).

SLAMF1 regulates TLR4-mediated signaling upstream of TBK1 and IRF3

Phosphorylation of IFN regulatory factor 3 (IRF3) transcription factor is critical for the regulation of early *IFNβ* transcription in macrophages (Sakaguchi et al., 2003). TBK1 acts upstream of IRF3 and phosphorylates IRF3 by itself or together with inhibitor of NF-κB kinase subunit ε (IKKε; Fitzgerald et al., 2003a). Macrophages silenced for SLAMF1 showed decreased levels in both LPS-induced TBK1 and IRF3 phosphorylation (Fig. 3, top). This was also observed in SLAMF1-silenced THP-1 cells stimulated with LPS or *E. coli* particles (Fig. S3, A and B).

Transcription of *IFNβ* is coordinately regulated by several transcription factor families such as IRFs, NF-κB, and ATF-2–c-Jun (Ford and Thanos, 2010). To explore events upstream of ATF-2–c-Jun activation, we analyzed the effect of SLAMF1 silencing on LPS-mediated activation of MAPKs. SLAMF1 silencing resulted in decreased phosphorylation of MAPK 7 (MAP3K)/TAK1 and downstream MAPKs (p38MAPK and JNK1/2; Figs. 3 and S3 A). Both p38MAPK and JNK1/2 positively regulate the transcriptional activity of AP1 (ATF-2–c-Jun; Chang and Karin, 2001), and it is therefore likely that the observed reduction in MAPK phosphorylation upon SLAMF1 silencing may contribute to decreased AP-1 activity.

The total level and phosphorylation of IκBα protein were not affected by LPS stimulation in the SLAMF1-depleted macrophages (Figs. 3 and S3 A, bottom), suggesting that SLAMF1 is not involved in the early NF-κB activation. This is consistent with our data showing that SLAMF1 silencing affected TNF levels only at late time points (Fig. 2, A–D).

To further support the hypothesis that SLAMF1 regulates signaling from the endosome leading to *IFNβ* expression, we transduced primary macrophages with lentiviruses encoding SLAMF1. LPS-mediated *IFNβ* mRNA expression was significantly higher in SLAMF1-transduced cells, with only a modest effect on *TNF* mRNA expression (Fig. 4 A). Western blot analysis showed that the upregulation of *IFNβ* mRNA expression in SLAMF1-transduced cells was accompanied by higher amounts of phosphorylated TBK1, IRF3, and MAPK phosphorylation

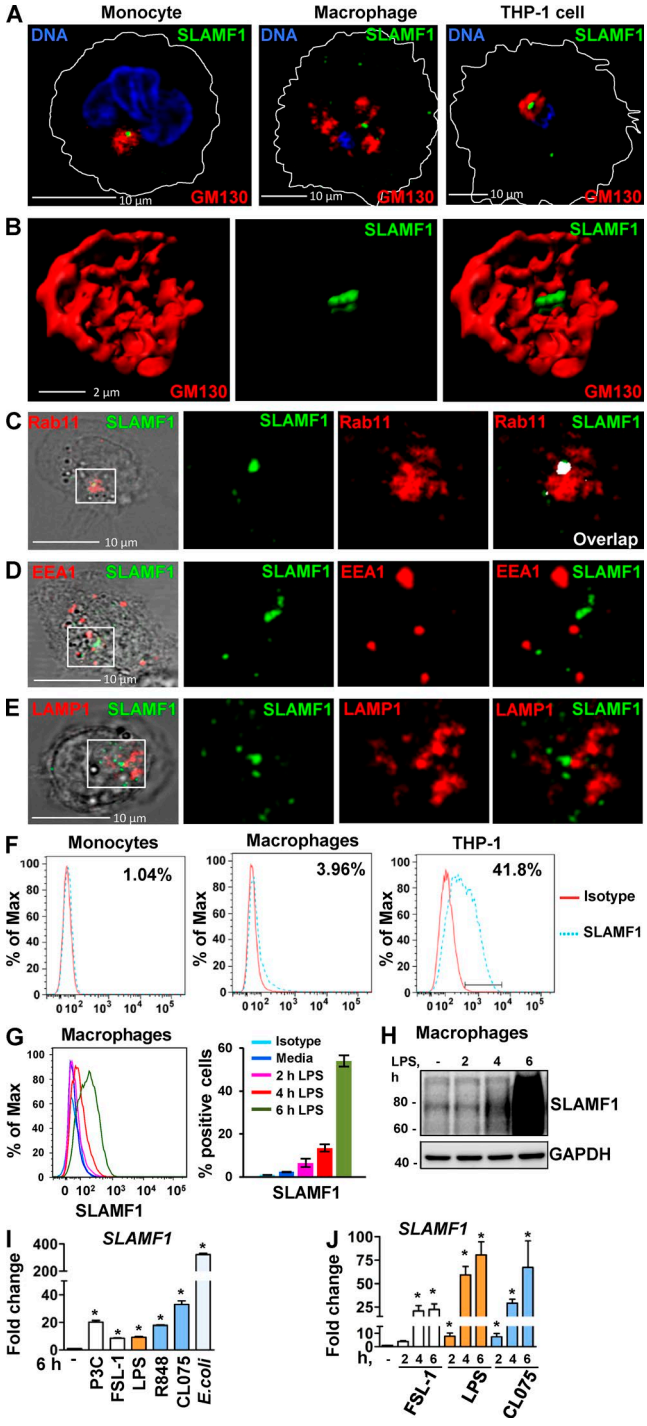

Figure 1. **SLAMF1 is enriched in the Rab11-positive ERCs in unstimulated macrophages, and SLAMF1 expression is induced by LPS and several other TLR ligands in primary human monocytes and macrophages. (A)** Monocytes, macrophages, and differentiated THP-1 cells stained with antibodies against SLAMF1 (green) and GM130 (red) and imaged by confocal microscopy. **(B)** 3D model of cis-Golgi (GM130) and SLAMF1 in THP-1 cells. Z stacks from the GM130 and SLAMF1 channels were obtained using high-resolution confocal microscopy followed by 3D modeling in IMARIS software. **(C)** Macrophages stained for SLAMF1 and Rab11 (ERC marker). Representative image. Overlapping pixels for SLAMF1 and Rab11 are shown in the white overlap. tM1 = 0.683 ± 0.08 (mean with SD) for z stacks of ERCs as ROIs (30 ROIs analyzed per donor) where tM1 was the Manders's colocalization coefficient with thresholds calculated in the Coloc 2 Fiji plugin with anti-SLAMF1 staining as first channel. **(D)** Macrophages costained for SLAMF1 and EEA1. **(E)** Macrophages costained for SLAMF1 and LAMP1. Colocalization accessed for z stacks for at least 30 cells for each experiment (four total) showing no colocalization for markers in both D and E. **(F)** Flow cytometry analysis of SLAMF1 surface expression by primary macrophages and differentiated THP-1 cells. Cells were costained for SLAMF1 and CD14 and gated for CD14-positive cells (primary cells) or stained for SLAMF1 (THP-1 cells). **(G)** Flow cytometry analysis of SLAMF1 surface expression by human macrophages stimulated by ultrapure K12 LPS (100 ng/ml) for 2, 4, and 6 h. **(H)** Western blot analysis of lysates from primary human macrophages stimulated by LPS for 2, 4, and 6 h. Graphs present mean values for three biological replicates with SD. Molecular weight is given in kilodaltons. **(I and J)** Quantification of *SLAMF1* mRNA expression by qPCR in monocytes (I) and macrophages (J) stimulated by TLRs' ligands FSL-1 (20 ng/ml), K12 LPS (100 ng/ml), and CL075 (1 µg/ml; both I and J) as well as R848 (1 µg/ml), Pam3Cys (P3C; 1 µg/ml), or K12 *E. coli* particles (20/cell; I only). Results are presented as means with SD. Statistical significance between groups was evaluated by a two-tailed *t* test. *, P < 0.01. Results are representative of at least four independent experiments/donors (A–H) or combined data for at least three donors (I and J).

(Fig. 4 B). Thus, these results also suggest that SLAMF1 acts as a positive regulator of endosomal TLR4–TRAM–TRIF signaling.

SLAMF1 regulates TRAM recruitment to *E. coli* phagosomes in a Rab11-dependent manner

Both TLR4 and TRAM are rapidly recruited to *E. coli* phagosomes after phagocytosis and are required for induction of IFNβ (Husebye et al., 2010). Because SLAMF1 was needed for TRAM-TRIF signaling, we tested whether SLAMF1 was recruited to *E. coli* phagosomes containing TRAM. We found that TRAM and SLAMF1 were recruited to early (EEA1-positive) and late (LAMP1-positive) *E. coli* phagosomes (Fig. 5 A). This was consistent with data published for SLAMF1 in mouse macrophages, where SLAMF1 was found both on EEA1- and LAMP1-positive *E. coli* phagosomes (Berger et al., 2010). Moreover, we did not detect SLAMF1 on *Staphylococcus aureus* phagosomes (Fig. S3, A and B), similar to data reported for mouse macrophages (Berger et al., 2010).

We hypothesized that SLAMF1 could be involved in the transport of TRAM to *E. coli* phagosomes as this is a crucial step for TLR4-dependent IFNβ induction. Control and SLAMF1-silenced macrophages were pulsed with *E. coli* pHrodo particles for 15 min followed by 15 min chase in particle-free medium. The mean voxel intensities (MIs) for TRAM, SLAMF1, and pHrodo fluorescence on the phagosomes were calculated from z stacks obtained by confocal microscopy using 3D image analysis software (Fig. 5 B). We found that uptake of *E. coli* particles was not significantly affected by SLAMF1 silencing (Fig. S4 C). However, acidification of the *E. coli* phagosomes was significantly decreased upon SLAMF1 silencing (Fig. S4 D). Remarkably, we found that TRAM recruitment to *E. coli* phagosomes was markedly decreased upon SLAMF1 silencing (Fig. 5 B, left). As expected, SLAMF1-silenced cells showed decreased amounts of SLAMF1 on *E. coli* phagosomes (Fig. 5 B, right). Thus, SLAMF1 seems to positively regulate TRAM recruitment to *E. coli* phagosomes.

Transport of TRAM to phagosomes is known to be Rab11 dependent (Husebye et al., 2010). Moreover, SLAMF1 was located to the Rab11-positive compartment in resting cells (Fig. 1 C), positively regulated transport of TRAM to phagosomes (Fig. 5 B), and relocalized from the ERC in monocytes upon addition of *E. coli* or LPS (Fig. S4, E–G). Based on these observations, we tested whether SLAMF1 recruitment

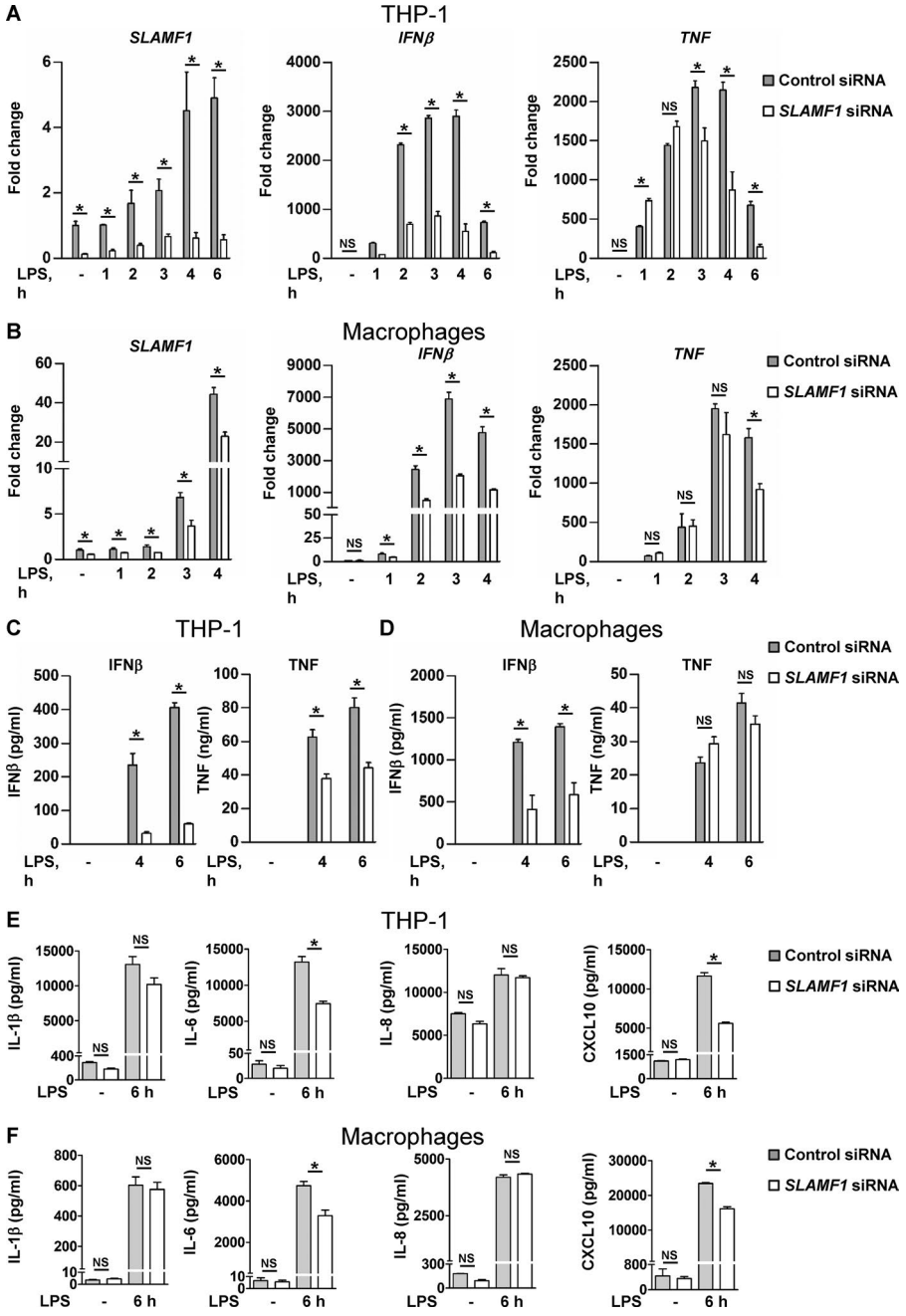

Figure 2. **Knockdown of SLAMF1 in macrophages results in strongly reduced TLR4-mediated *IFNβ* mRNA expression and protein secretion as well as some decrease of TNF, IL-6, and CXCL10 secretion. (A and B)** Quantification of *SLAMF1*, *IFNβ*, and *TNF* mRNA expression by qPCR in THP-1 cells (A) and macrophages (B) treated by 100 ng/ml ultrapure K12 LPS. **(C and D)** IFNβ and TNF secretion levels by THP-1 cells (C) and macrophages (D) in response to LPS (4 and 6 h) assessed by ELISA. **(E and F)** Secretion levels of IL-1β, IL-6, IL-8, and CXCL-10 (6 h LPS) analyzed by multiplex assays. Data are presented as means with SD for combined data from three independent experiments (A, C, and E), for three biological replicates from one of six donors (B and D), or one of three donors (F). *, $P < 0.01$.

to phagosomes was Rab11 dependent. Two members of Rab11 subfamily, Rab11a and Rab11b, were simultaneously silenced in human macrophages. After silencing, macrophages were stimulated with *E. coli* for 15 and 30 min, and recruitment of TRAM and SLAMF1 to the phagosomes was quantified by evaluating MIs for TRAM and SLAMF1 staining (Fig. 5 C). Rab11 silencing significantly reduced the amounts of SLAMF1 and TRAM at the phagosomes (Fig. 5 C).

SLAMF1 interacts with the N-terminal part of the TRAM TIR domain

To investigate whether TRAM recruitment to *E. coli* phagosomes could be regulated by a physical interaction between SLAMF1 and TRAM, we performed endogenous immunoprecipitations (IPs) using anti-SLAMF1 and anti-TRAM antibodies. Endogenous SLAMF1 coprecipitated with TRAM in macrophages, and this interaction was enhanced upon LPS stimulation (Fig. 6 A). In contrast, the TIR-adapter MyD88 did not coprecipitate with SLAMF1 (Fig. 6 A, right), supporting the specificity of the SLAMF1–TRAM interaction. Endogenous TRAM also coprecipitated with SLAMF1 both before and after LPS treatment (Fig. 6 B). The bands detected by anti-TRAM antibody were specific as a similar band could be observed in coimmunoprecipitations (co-IPs) with TLR4 upon LPS stimulation (Fig. S5 A). Overall, we conclude that endogenous SLAMF1 interacts with TRAM in human macrophages and that the interaction is enhanced upon LPS stimulation.

Furthermore, HEK293T cells were transiently transfected with Flag-tagged TRAM ($TRAM^{Flag}$) and full-length SLAMF1 or deletion mutant lacking the C terminus of SLAMF1 (SLAMF1Δct). We found that full-length SLAMF1 but not

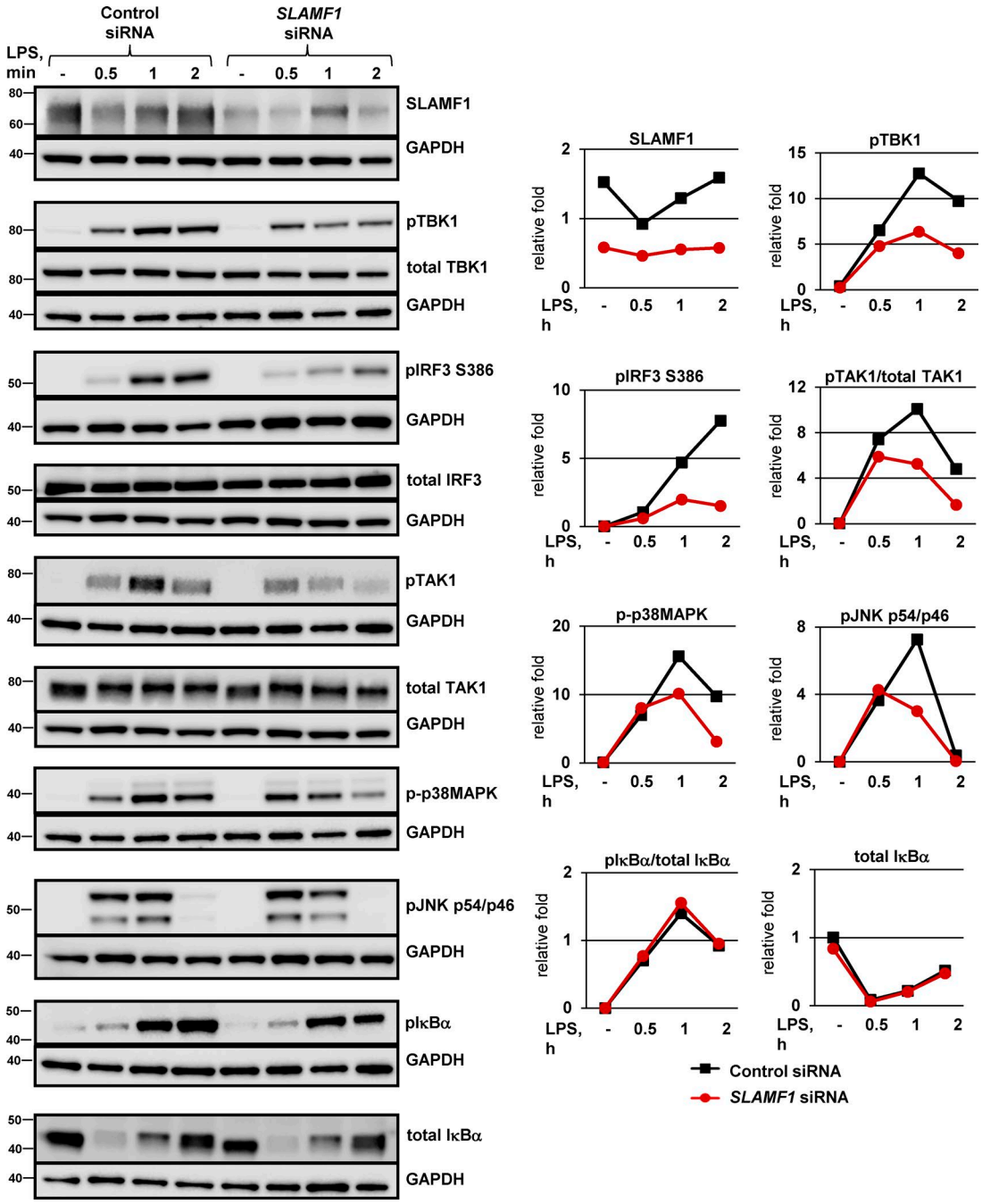

Figure 3. **SLAMF1 silencing in macrophages impairs TLR4-mediated phosphorylation of TBK1, IRF3, and TAK1.** Western blotting of lysate macrophages treated with a control nonsilencing oligonucleotide or *SLAMF1*-specific siRNA oligonucleotides and stimulated with 100 ng/ml LPS. The antibodies used are indicated in the figure. An antibody toward SLAMF1 was used to control for SLAMF1 silencing, and GAPDH was used as an equal loading control. Same GAPDH controls are presented for pTBK1, total TBK1, and phospho-p38MAPK, for total IRF3 and total TAK1, and for pTAK1 and pIκBα because they were probed on the same membranes. Western blots are representative of one of five donors. Molecular weight is given in kilodaltons. Graphs (right) show quantifications of protein levels relative to GAPDH levels obtained with Odyssey software.

SLAMF1Δct coprecipitated with TRAM^{Flag}, suggesting that the TRAM interaction site was located at the C terminus of SLAMF1 protein (Fig. 6 C). To map the TRAM region responsible for the interaction with SLAMF1, we generated several Flag-tagged TRAM deletion mutants. The mutants contained the N terminus (1–68), C terminus (158–225), TIR domain (68–176), or the TIR domain plus the C terminus (68–235) of TRAM (1–235; UniProtKB, Q86XR7). Of all these mutants, only TRAM 68–235 and TRAM 68–176 coprecipitated with SLAMF1 (Fig. 6 D).

To further define the subdomain of TRAM involved in the TRAM–SLAMF1 interaction, we made a series of TRAM deletion mutants, which contained the N-terminal part of TRAM with 10–20-aa increments. Although TRAM 1–68 mutant did not bind SLAMF1 (Fig. 6, D and E), a weak interaction was found with TRAM 1–79 that increased markedly for TRAM 1–90 and further for TRAM 1–100. Collectively, these results suggest that the SLAMF1 binding site in TRAM is located within the first 30–35 aa of the TRAM TIR domain (68–95 aa; Fig. 6 E).

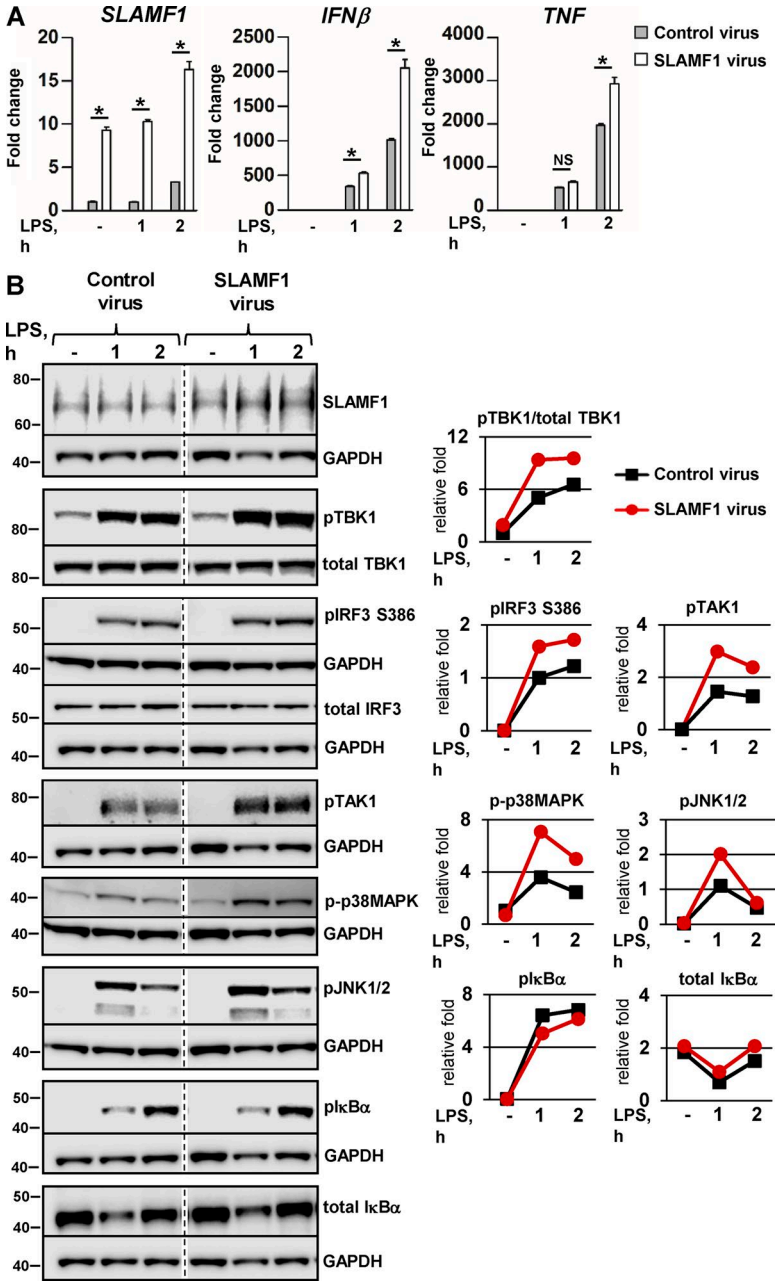

Figure 4. **Lentiviral transduction of SLAMF1 in macrophages results in the increase of IRF3 and TBK1 phosphorylation in response to LPS and upregulation of IFNβ and TNF expression. (A)** Quantification of *SLAMF1*, *IFNβ*, and *TNF* mRNA expression by qPCR in macrophages transduced by Flag-tagged SLAMF1 coding or control virus and treated by LPS. The qPCR data are presented as means and SD for three biological replicates of one of three experiments. Significance was calculated by two-tailed *t* tests. *, $P < 0.01$. **(B)** Western blots showing LPS-induced phosphorylation of signaling molecules in cells transduced with the SLAMF1-expressing virus versus control virus. Dividing lines were added where the time point of 4 h was excised. The same GAPDH controls are presented for total IRF3 and total IκBα and for pIκBα and pTAK1 because they were probed on the same membranes. Molecular weight is given in kilodaltons. Graphs (right) show quantifications of protein levels relative to GAPDH levels obtained with Odyssey software.

TRAM interacts with the C-terminal part of SLAMF1, and the interaction occurs for human but not mouse proteins

We used a similar strategy to establish the TRAM-interacting subdomain of SLAMF1 by deleting amino acids from the C-terminal part of SLAMF1. Cells were cotransfected with Flag-tagged SLAMF1 WT or deletion mutants along with $TRAM^{YFP}$ (Fig. 6 F). A deletion mutant (1–330) lacking the last five C-terminal amino acids did not interact with $TRAM^{YFP}$ (Fig. 6 F), pinpointing the TRAM interaction site at the very C terminus of SLAMF1.

There are two tyrosine residues in the cytoplasmic tail of human SLAMF1 in the signaling motifs designated as immunoreceptor tyrosine–based switch motifs (Shlapatska et al., 2001). SLAMF1 tyrosine phosphorylation and interaction with other proteins via immunoreceptor tyrosine–based switch motifs could potentially alter SLAMF1–TRAM interaction. Point mutations Y281F, Y327F, and double mutation Y281/327F did not alter the interaction with TRAM (Fig. S5 B). Endogenous SLAMF1 was tyrosine phosphorylated in resting macrophages and subsequently dephosphorylated within the 45 min of LPS stimulation (Fig. S5, C and D). Furthermore, both nonphosphorylated and tyrosine-phosphorylated (pY) recombinant SLAMF1ct GST fusion proteins effectively pulled out TRAM from lysates of untreated or LPS-treated macrophages (Fig. S5 E). Thus, SLAMF1–TRAM interaction was not altered by tyrosine phosphorylation of SLAMF1.

Regulation of the LPS-induced IFNβ response seems to differ between humans and mice. Human macrophages respond to LPS with at least 10-fold higher *IFNβ* mRNA expression compared with mouse BMDMs and thioglycolate-elicited peritoneal macrophages (Schroder et al., 2012). Thus, we wanted to check whether SLAMF1 and TRAM interaction was conserved across species, and we tested murine SLAMF1 and TRAM proteins for interaction. Indeed, mouse $TRAM^{EGFP}$ did not coprecipitate with mouse $SLAMF1^{Flag}$ (Fig. 6 G). Interestingly,

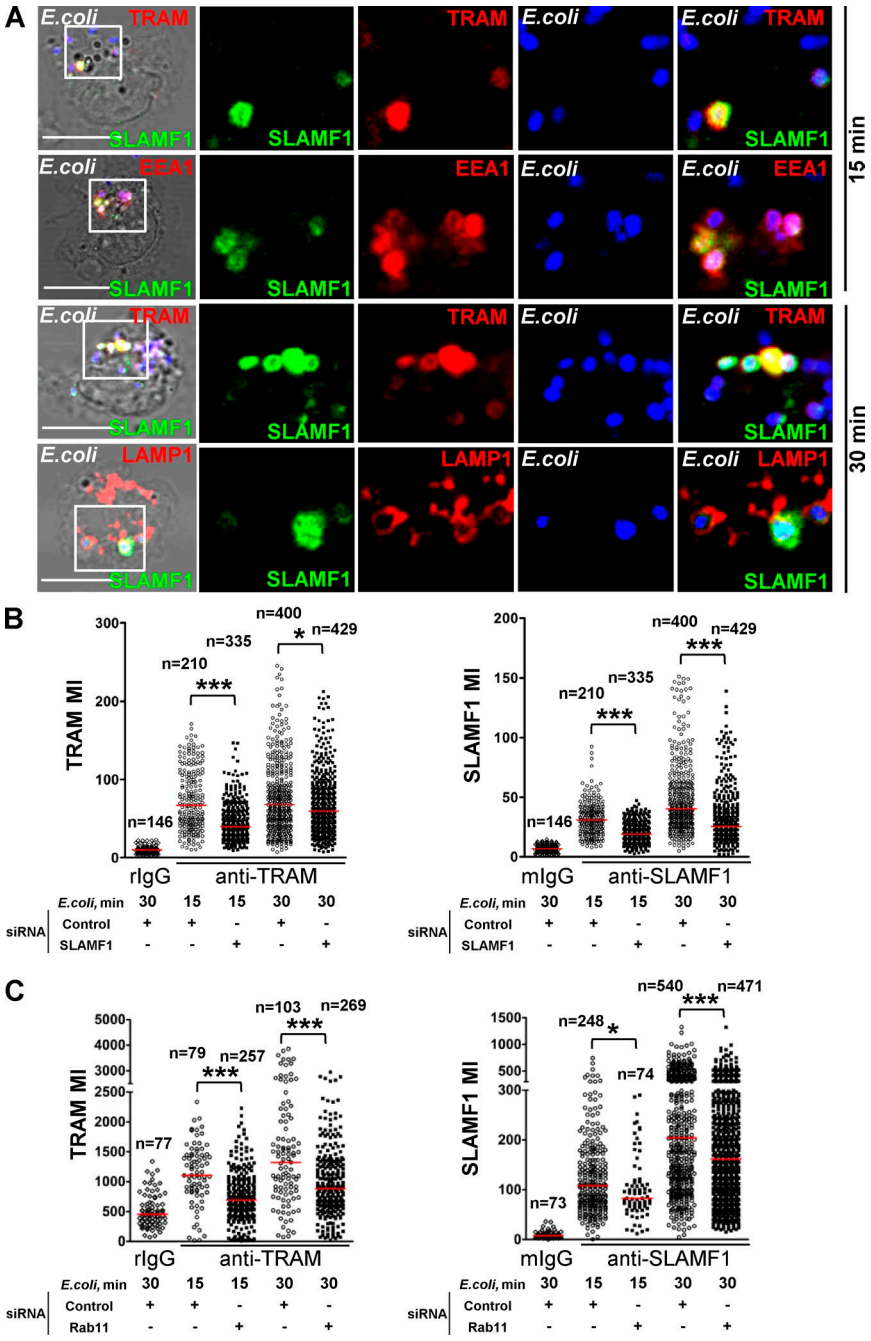

Figure 5. **SLAMF1 regulates TRAM recruitment to *E. coli* phagosomes. (A)** SLAMF1 costaining with TRAM, EEA1, or LAMP1 in primary macrophages coincubated with *E. coli* pHrodo particles for indicated time points. SLAMF1 (green), *E. coli* (blue), and TRAM, EEA1, or LAMP1 (red) are shown. The data shown are representative of one out of four donors. Bars, 10 µm. **(B and C)** TRAM and SLAMF1 MIs on *E. coli* phagosomes upon SLAMF1 silencing (B) or simultaneous Rab11a and Rab11b silencing (C) in primary human macrophages quantified from xyz images. The scatter plots are presented as median values of TRAM voxel intensity, and numbers of phagosomes are shown at the top. The nonparametric Mann-Whitney test was used to evaluate statistical significance. *, $P < 0.01$; ***, $P \leq 0.0001$. Human macrophages were incubated with *E. coli* particles for indicated time points, fixed, and costained for SLAMF1 and TRAM, normal rabbit (rIgG), or mouse IgG (mIgG). The data shown are representative for one out of five (B) or four (C) donors.

three amino acids in human SLAMF1ct upstream of potential TRAM-binding site TNSI (321–324; UniProtKB, Q13291) are different from mouse SLAMF1ct, containing PNPT (329–332; UniProtKB, Q9QUM4; Fig. S6 A). Substitution of the TNSI sequence with PNPT in human SLAMF1 abrogated its interaction with $TRAM^{YFP}$ (Fig. 6 H). Thus, these amino acids are crucial for interaction. However, the sequence in human TRAM involved in the interaction with human SLAMF1 is not fully conserved in murine TRAM (Fig. S6 B), which also could explain why murine TRAM and SLAMF1 do not interact.

SLAMF1 has been shown to regulate *E. coli* phagosome maturation in mouse BMDMs, but it did not modify the response to ultrapure LPS (Berger et al., 2010). However, regulation of mRNA expression or secretion of type I IFNs by SLAMF1 have not been previously addressed in BMDMs. We stimulated C57BL/6 *Slamf1*$^{-/-}$ and control BMDMs with 100 ng/ml of ultrapure LPS or *E. coli* particles and tested for *Ifnβ* and *Tnf* mRNA expression and cytokine secretion (Fig. S6, C–E). Indeed, *Slamf1*$^{-/-}$ BMDMs showed comparable *Ifnβ* and *Tnf* mRNA levels to control BMDMs (Fig. S5 C), and the amounts of IFNβ and TNF secreted from *Slamf1*$^{-/-}$ BMDMs stimulated with LPS or *E. coli* were not significantly altered (Fig. S6, D and E). Thus, mouse SLAMF1 does not interact with TRAM protein. Therefore, mouse SLAMF1 did not affect TRAM-TRIF–mediated IFNβ secretion in murine macrophages.

Rab11 interacts with SLAMF1 via class I FIPs

As SLAMF1 recruitment to *E. coli* phagosomes was found to be Rab11 dependent (Fig. 5 C), we investigated whether

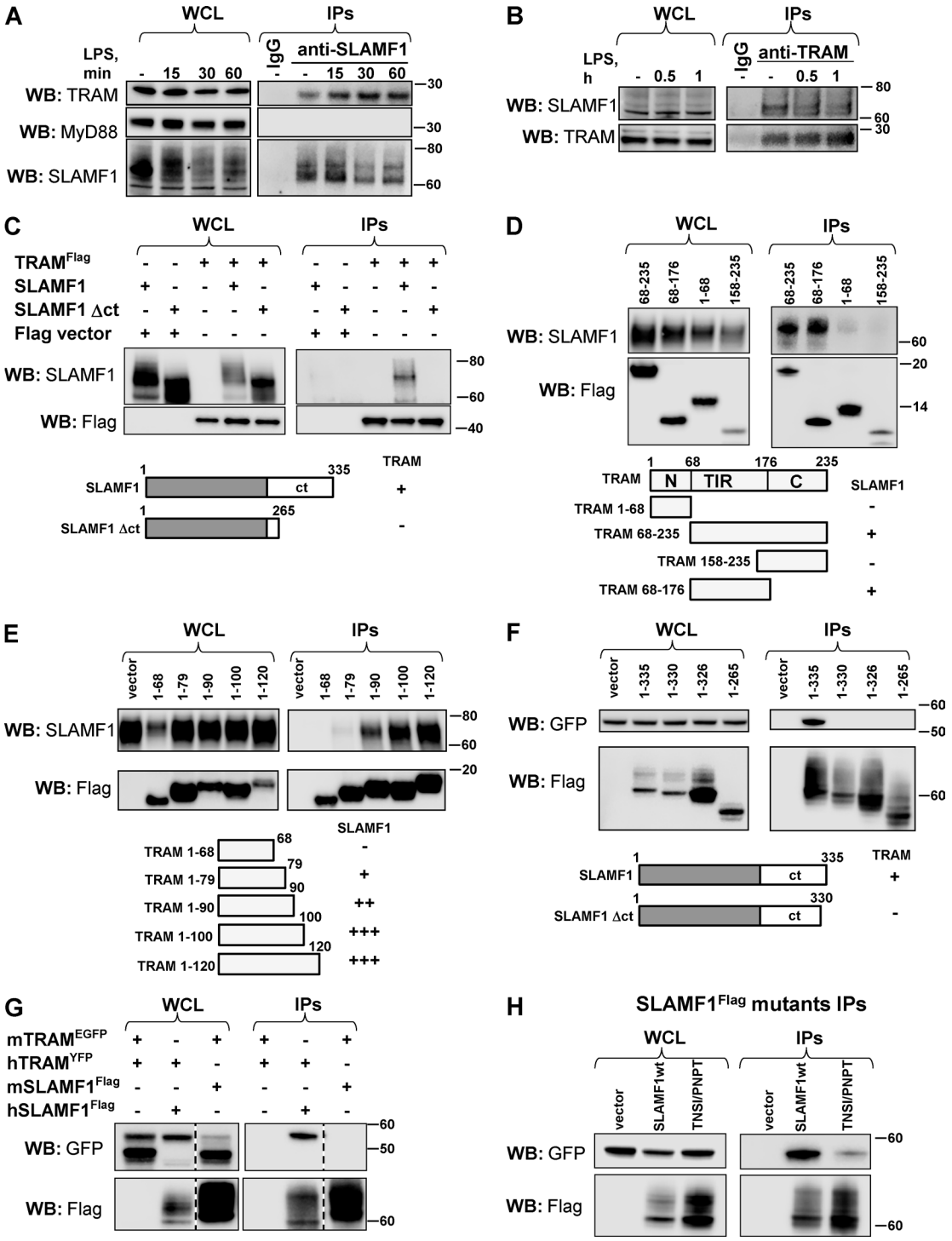

Figure 6. **SLAMF1 interacts with TRAM protein. (A)** Endogenous IPs using specific anti-SLAMF1 mAbs from macrophages stimulated by LPS. **(B)** Endogenous IPs using anti-TRAM polyclonal antibodies from macrophages stimulated by LPS. **(C)** TRAM^{Flag}-precipitated SLAMF1 and SLAMF1ct was needed for interaction with TRAM. **(D)** Coprecipitation of TRAM deletion mutants: TIR domain (68–235), short TRAM TIR domain (68–176 aa), and N-terminal (1–68 aa) or C-terminal (158–235 aa) domains with SLAMF1 protein. **(E)** Coprecipitation of TRAM deletion mutants containing the N-terminal part of TRAM TIR domain with SLAMF1. **(F)** Coprecipitation of SLAMF1^{Flag} deletion mutants with TRAM^{YFP}. **(G)** Coprecipitation of human SLAMF1^{Flag} with human TRAM^{YFP} and of mouse SLAMF1^{Flag} with mouse TRAM^{EGFP}. Black dashed lines indicate that intervening lanes have been spliced out. **(H)** Human SLAMF1 cytoplasmic tail coprecipitation with TRAM^{YFP} with or without amino acid substitutions at 321–324. Graphs under C–F summarize the IPs' results. Indicated constructs were transfected to HEK293T cells, and anti-Flag agarose was used for the IPs. For endogenous IPs, specific SLAMF1 or TRAM antibodies were covalently coupled to beads. At least three independent experiments were carried out for anti-Flag IPs, and five independent experiments were carried out for the endogenous IPs, and one representative experiment is shown for each. Molecular weight is given in kilodaltons. WB, Western blot; WCL, whole-cell lysate.

SLAMF1 could form a complex with Rab11 via effector proteins such as Rab11 FIPs (Horgan and McCaffrey, 2009). Individual FIPs (FIP1–5) were coexpressed together with SLAMF1 and Rab11a^{Flag} proteins in HEK cells followed by co-IP with Rab11a^{Flag} (Fig. 7 A). All three members of class I FIPs were found to form a complex with SLAMF1 and Rab11a (Fig. 7 A). All class I FIPs are characterized by a phospholipid-binding C2 domain (Fig. 7 B), which is located between aa 1–129 in FIP2 (Lindsay and McCaffrey, 2004). We found that the ΔC2 mutant of FIP2 (lacking aa 1–128) could still bind SLAMF1 (Fig. 7 D). Protein sequence alignment between the class I FIPs showed a highly conserved domain between aa 117–191 in FIP2 with undefined function (Fig. 7, B and C). To figure out whether this domain in FIP2 could be responsible for interaction with SLAMF1, several Flag-tagged FIP2 deletion mutants were tested with or without Rab11^{CFP} overexpression. The 1–192-aa deletion mutant was the minimal deletion mutant found to interact with SLAMF1 (Fig. 7, D–F). Both this mutant and the ΔC2 mutant contains a common 62-aa motif that could be important for interaction with SLAMF1 (Fig. 7, D–F).

The tested deletion mutants more efficiently precipitated SLAMF1 than the full-length FIP2 (Fig. 7 E), but coexpression of Rab11 with full-length FIP2 and SLAMF1 markedly increased its binding to SLAMF1 (Fig. 7, F and G). All FIP2 deletion mutants in IPs lacked a C-terminal Rab11 binding domain (Fig. 7, B, E, and F) and showed better coprecipitation with SLAMF1 without Rab11 overexpression, which suggested that Rab11 has a critical role in controlling FIP2–SLAMF1 interactions.

Next, we examined whether FIPs could coprecipitate SLAMF1 efficiently only in the presence of GTP-bound active Rab11. Rab11 GTPase functions as a molecular switch, being active in the GTP-bound state and inactive in the GDP-bound state. It has been shown that FIPs only interact with activated Rab11 (Junutula et al., 2004; Gidon et al., 2012). FIP2^{Flag} was precipitated from cells, which coexpressed SLAMF1 with either Rab11a WT, GTP-bound Rab11Q70L, or GDP-bound Rab11a S25N (Fig. 7 G). FIP2^{Flag} coprecipitated with SLAMF1 only in the presence of Rab11 WT and Rab11Q70L but not Rab11 serine mutant (Fig. 7 G). We also found that the interaction domain for FIP2 in SLAMF1ct was distinctly different from the TRAM interaction domain (Figs. 6 F and 7, I and J). Our results suggest that TLR4-induced activation of Rab11 is a signal for the recruitment of SLAMF1 and TRAM via the FIPs to *E. coli* phagosomes and that class I FIPs may link the SLAMF1–TRAM complex to Rab11.

SLAMF1 is recruited to the TLR4–TRAM–TRIF complex

We defined the SLAMF1-interacting site in TRAM as the N-terminal part of TRAM TIR domain (68–95 aa; Fig. 6 C). This raised an important question of whether SLAMF1 could regulate the subsequent formation of TLR4–TRAM–TRIF complex needed for LPS-mediated signaling. To address this question, HEK cells were cotransfected by SLAMF1^{Flag}, TRAM^{YFP}, and TLR4^{Cherry} or TRIF^{HA}, and their interactions were monitored by co-IP with SLAMF1^{Flag}. Both TLR4^{Cherry} and TRIF^{HA} coprecipitated with SLAMF1^{Flag} in the presence of TRAM^{YFP} (Fig. 8, A and B). In addition, SLAMF1 did not coprecipitate with TLR4^{Flag} in the absence of TRAM^{YFP} (Fig. 8 C). Overexpression of SLAMF1 did not alter the ability of TLR4 to attract TRIF via TRAM despite that SLAMF1 also coprecipitated with the complex in the presence of TRAM and TRIF (Fig. 8 D). Furthermore, TRIF overexpression strongly enhanced SLAMF1 coprecipitation with TLR4^{Flag} (Fig. 8 E). In summary, SLAMF1 binding to TRAM seems to be unique and outside of the TIR-TIR dimerization domain as it does not interfere with TRAM–TLR4 interaction and subsequent TRIF recruitment.

TRAM and SLAMF1 positively regulate bacterial killing by macrophages

SLAMF1 controls killing of Gram-negative bacteria by mouse BMDMs through generation of ROS (Berger et al., 2010). We tested *E. coli*–mediated ROS generation by *SLAMF1*-silenced human macrophages and found that SLAMF1 also acts as a positive regulator of ROS generation in human cells (Fig. 9 A).

Slamf1$^{-/-}$ BMDMs demonstrated reduced bacterial killing at 6 h of *E. coli* infection (Berger et al., 2010). To test the effect of SLAMF1 on bacterial killing by human cells, *SLAMF1*-silenced THP-1 or TRAM knockout (KO) cells with respective control cells were incubated with live DH5α *E. coli*. Bacterial killing was strongly decreased already at early time points (1 h and 1.5 h) in SLAMF1-silenced cells (Fig. 9 B) and was almost completely abolished in TRAM KO cells (Fig. 9 C). Negative values of the percentage of killing in TRAM KO cells pointed to intracellular bacterial replication in these cells (Fig. 9 C).

TRIF-dependent signaling activates TBK1-IKKε kinases that regulate the integrity of pathogen-containing vacuoles and restrict bacterial proliferation in the cytosol (Radtke et al., 2007; Thurston et al., 2016). TRAM is a crucial adapter for TRIF recruitment to activated TLR4, leading to the activation of TBK1 and IKKε (Oshiumi et al., 2003; Yamamoto et al., 2003; Fitzgerald et al., 2004). Upon TLR4 ligation, TBK1 and IKKε phosphorylate Akt kinase (S473), resulting in Akt activation (Krawczyk et al., 2010; Everts et al., 2014). In turn, the Akt-mTORC1 signaling axis can drive phagocytosis, phagosome maturation, and ROS production, which are essential for bacterial killing (Kelly and O'Neill, 2015). As expected, TRAM KO cells had no detectable IRF3 phosphorylation in response to *E. coli* particles (Fig. 9 D). In control cells, *E. coli*–mediated Akt S473 phosphorylation underwent the similar kinetics as IRF3 phosphorylation and was completely abolished in TRAM KO cells (Fig. 9 D) and strongly decreased in SLAMF1-depleted cells (Fig. 9 E). The TBK1-IKKε inhibitor MRT67307 decreased TLR4-mediated Akt phosphorylation in THP-1 cells, whereas the Akt inhibitor MK2206 completely abrogated Akt phosphorylation (Fig. 9 F). Both compounds inhibited bacterial killing in THP-1 cells, especially at the earliest time point (Fig. 9 G). Moreover, coincubation with MRT67307 resulted in the increase of intracellular bacterial number as could be seen by negative values in the percentage of bacterial killing (Fig. 9 G). Hence, TBK1-IKKε activity and subsequent *E. coli*–mediated Akt phosphorylation directly correlated with the ability of cells to kill bacteria and restrict intracellular replication.

Activation of PI3K and subsequent Akt phosphorylation downstream of TLR2 and TLR4 has been extensively explored in many model systems (Laird et al., 2009; Troutman et al., 2012). It was previously reported that TLR2- and TLR4-mediated Akt S473 phosphorylation is MyD88 dependent in murine model systems (Laird et al., 2009). Our data on MyD88 silencing in primary human macrophages showed that *E. coli*–induced Akt S473 phosphorylation was not dependent on MyD88 but was dependent on TRAM (Fig. S7 A). In human macrophages, the kinetics of Akt phosphorylation induced by *E. coli* particles were much faster and robust than those induced

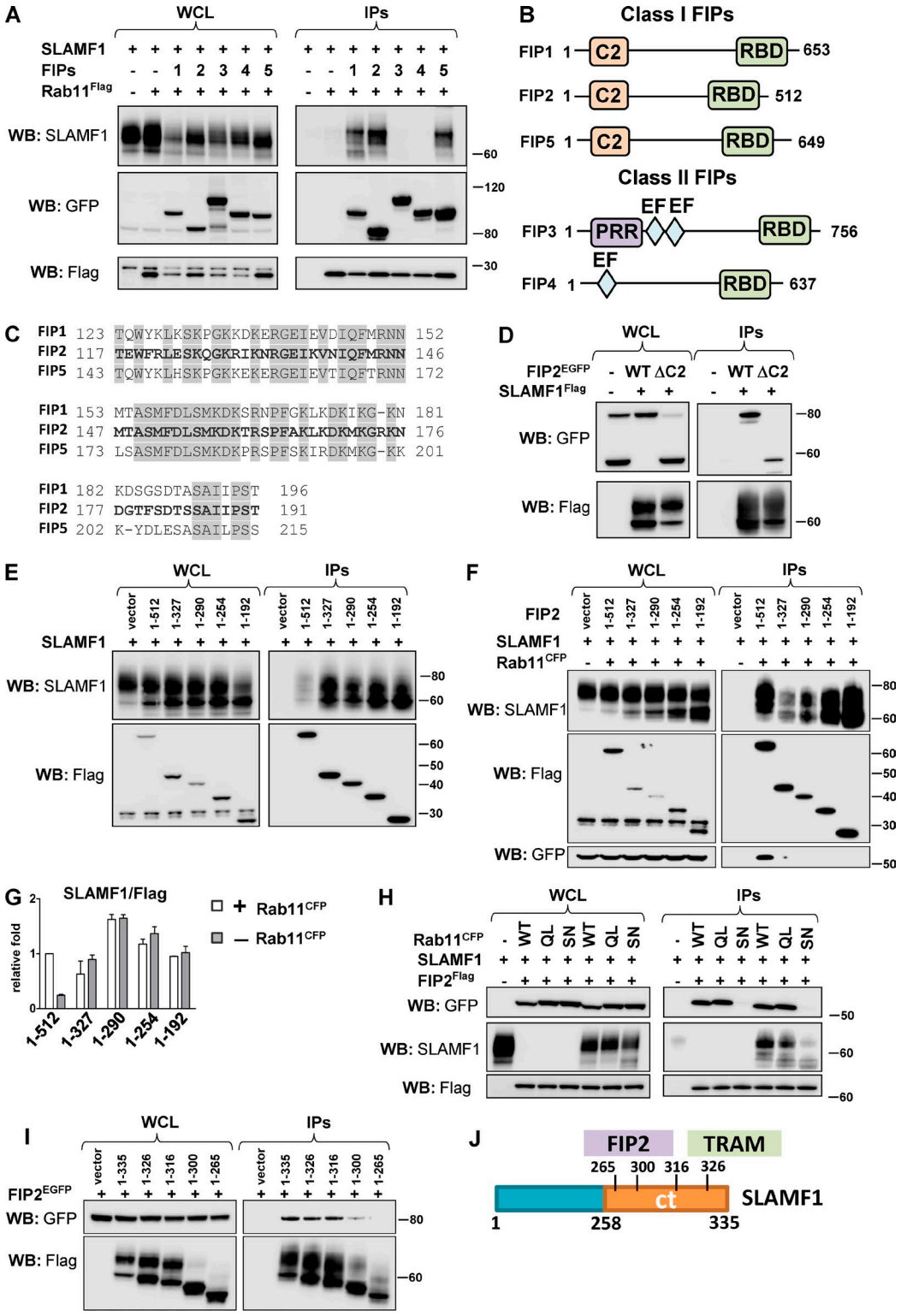

Figure 7. **SLAMF1 interacts with all class I Rab11 FIPs. (A)** Anti-Flag IPs for Rab11a^{Flag} with EGFP-tagged Rab11FIPs (1–5) and SLAMF1. **(B)** Schematic figure for class I and class II Rab11 FIPs domain structure. C2, phospholipid-binding C2 domain; EF, EF-hand domain; PRR, proline-rich region; RBD, Rab11 binding domain. **(C)** Homologous protein sequence in class I FIPs, which follow the C2 domain. Identical amino acids in all three class I FIPs are highlighted. **(D)** Coprecipitation of SLAMF1^{Flag} with FIP2^{EGFP} WT or FIP2 deletion mutant lacking the C2 domain (ΔC2). **(E and F)** Coprecipitation of untagged SLAMF1 with FIP2^{Flag} (1–512 aa) and Flag-tagged FIP2 deletion mutants in anti-Flag IPs in the absence (E) or presence (F) of overexpressed Rab11^{CFP}. **(G)** Quantification of coprecipitations in E and F between SLAMF1 and FIP2^{Flag} variants correlated with the amount of Flag-tagged protein on the blot and Flag-tagged protein sizes. Error bars represent means ± SD for three independent experiments. **(H)** Coprecipitation of FIP2^{Flag} with SLAMF1 and Rab11a WT, Rab11a Q70L mutant (QL), or Rab11a S25N mutant (SN). **(I)** Coprecipitation of SLAMF1^{Flag} deletion mutants with FIP2^{EGFP}. Molecular weight is given in kilodaltons. WB, Western blot; WCL, whole-cell lysate. **(J)** Scheme for FIP2- and TRAM-interacting domains in SLAMF1ct. The results are representative of at least three independent experiments.

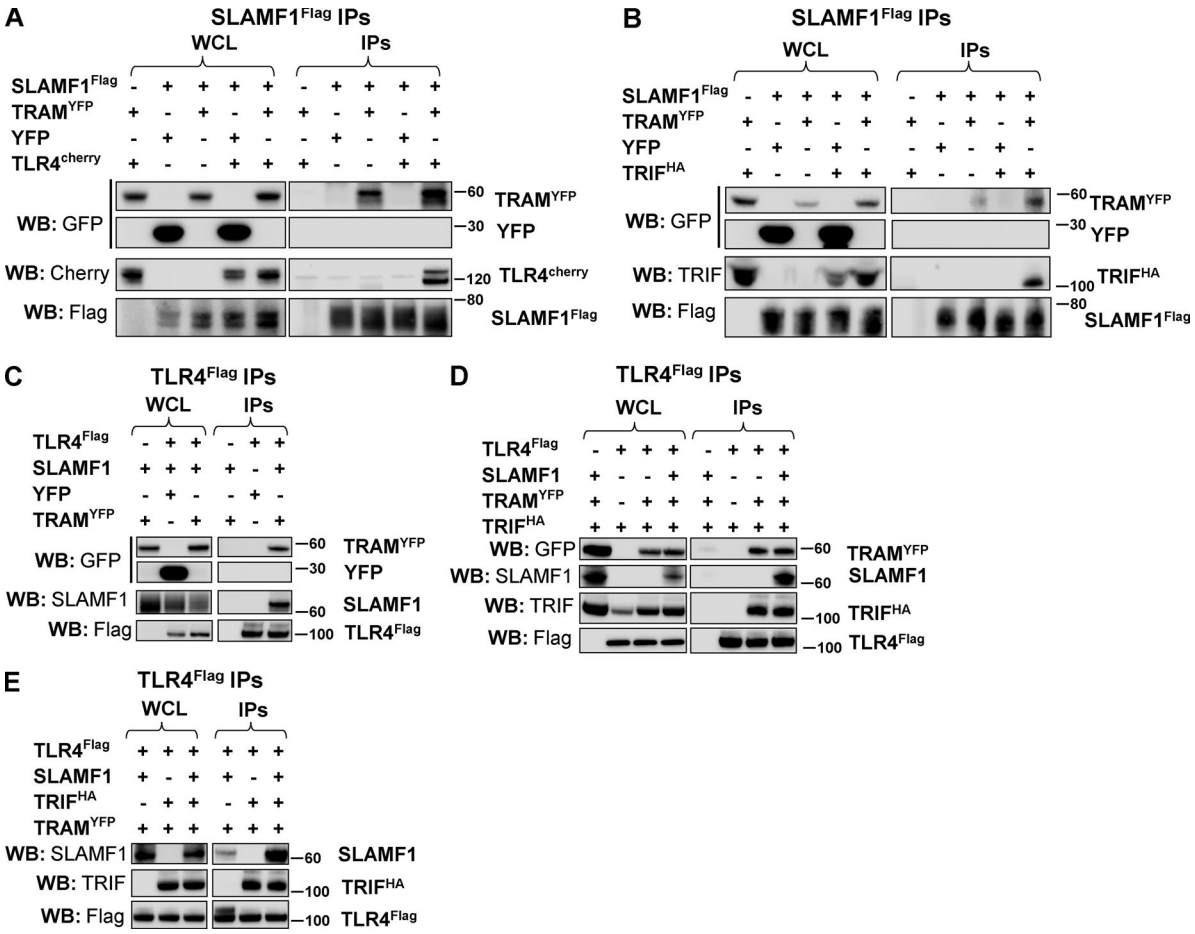

Figure 8. **TRAM acts as a bridge between the SLAMF1 and TLR4 signaling complex. (A and B)** Coprecipitations of SLAMF1^{Flag} with TLR4^{Cherry} (A) or TRIF^{HA} (B) with or without TRAM^{YFP} overexpression. **(C)** Coprecipitation of TLR4^{Flag} with SLAMF1 with or without TRAM^{YFP} overexpression. **(D)** TLR4^{Flag} interaction with TRAM^{YFP} and TRIF^{HA} with or without SLAMF1 coexpression. **(E)** Coprecipitation of SLAMF1 with or without TRIF^{HA} in the presence of TRAM^{YFP} by TLR4^{Flag}. Indicated constructs were transfected to HEK293T cells. pDuo-CD14/MD-2 vector was cotransfected to all wells (A and C–E). Anti-Flag agarose was used for IPs. At least three independent experiments were performed. Molecular weight is given in kilodaltons. WB, Western blot; WCL, whole-cell lysate.

by the TLR2 ligand FSL-1 or the TLR4 ligand LPS (Fig. S7 B). TLR2 and TLR4 ligands were not inducing pAkt much over the background level in THP-1 cells, which were used for bacterial killing assays, and pAkt levels were only modestly affected by *SLAMF1* or *TRAM* silencing (Fig. S7 C). In contrast, THP-1 cells stimulated with *E. coli* particles showed a 15–20-fold increase in pAkt that were almost lost in cells depleted for *TRAM* or *SLAMF1* (Fig. 9, D and E). Thus, TRAM and SLAMF1 are involved in regulation of *E. coli*–mediated but not pure TLR ligand–mediated Akt phosphorylation in THP-1 cells.

Discussion

Despite that SLAMF1 has been reported to control inflammatory responses and defense against Gram-negative bacteria in mice, the underlying mechanisms are elusive (Theil et al., 2005; van Driel et al., 2012, 2016). Moreover, little has been shown about the role of SLAMF1 in modulating the inflammatory response against Gram-negative bacteria in human macrophages. In this study, we show for the first time that human SLAMF1 regulates TLR4-mediated TRAM-TRIF–dependent signaling by the unique interaction with the signaling adapter TRAM.

Mouse BMDMs express high levels of SLAMF1 on the plasma membrane, whereas resting human monocytes and human monocyte–derived macrophages have been considered to be SLAMF1 negative (Farina et al., 2004; Romero et al., 2004). In contrast, we found that human monocytes and macrophages largely expressed SLAMF1 in the intracellular Rab11^{+} ERC compartment; however, they had weak or no expression on the cell surface. After stimulation by *E. coli*, SLAMF1 relocalized from ERCs to *E. coli*– or LPS-containing phagosomes that resembled the previously reported Rab11a-dependent transport of TLR4 and TRAM from ERCs to *E. coli* phagosomes (Husebye et al., 2010). Endogenous SLAMF1 was already bound to TRAM before stimulation, and upon *E. coli* phagocytosis, both proteins were recruited to phagosomes by Rab11 GTPases, with class I Rab11 FIPs as effector molecules. It is known that Rab11 functions as a molecular switch, which cycles between two conformational states: a GTP-bound "active" form and a GDP-bound "inactive" form (Guichard et al., 2014). Surface TLR4 interaction with LPS on the *E. coli* outer membrane induces fast intracellular complex formation, resulting in multiple post-

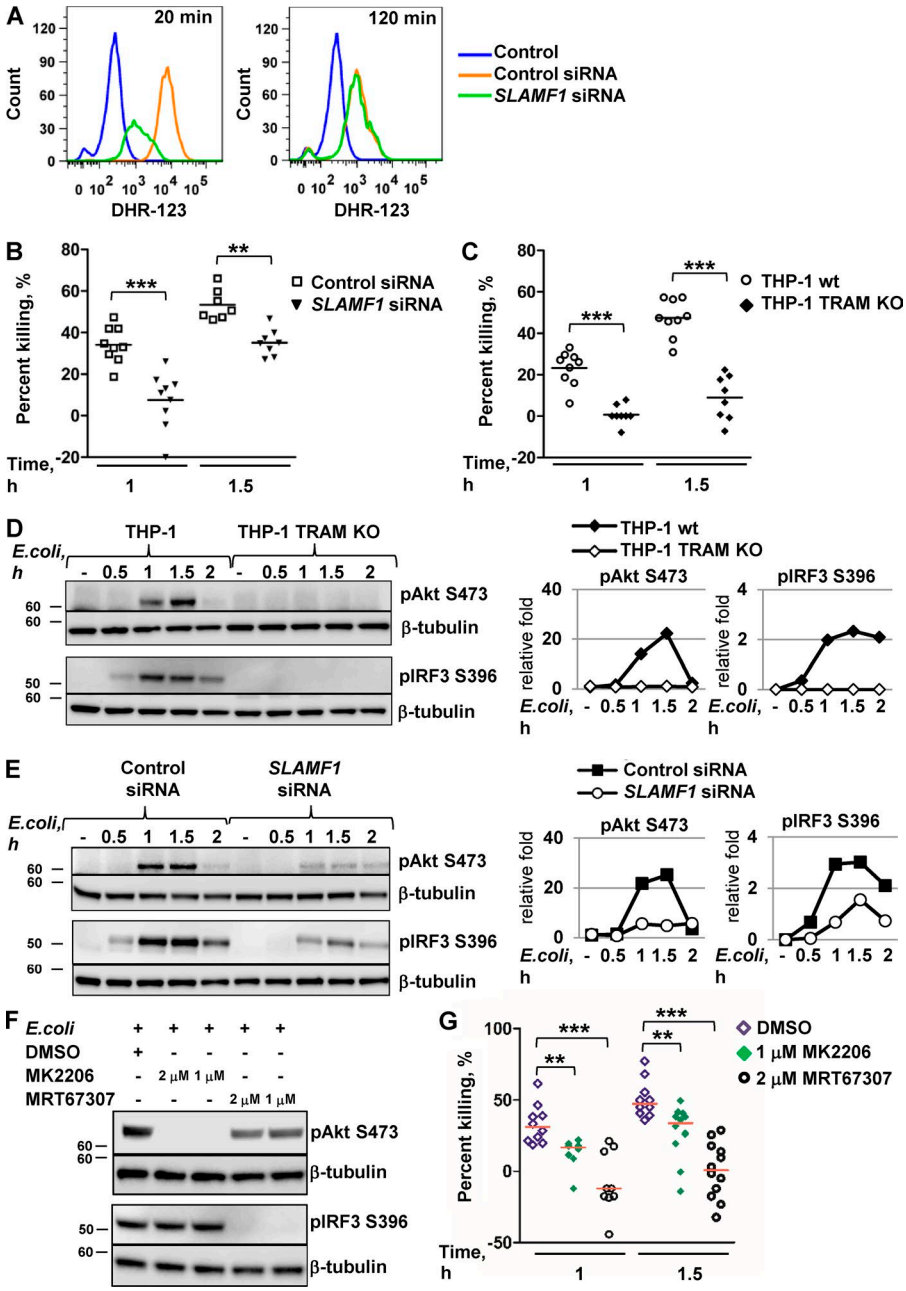

Figure 9. **TRAM and SLAMF1 are essential for the killing of *E. coli* by human macrophages. (A)** Flow cytometry analysis of dihydrorhodamine 123 (DHR-123) fluorescence to access ROS activation in control siRNA or *SLAMF1* siRNA human macrophages upon stimulation by *E. coli* red pHrodo particles. One of three experiments shown. **(B and C)** Bacterial killing assays by SLAMF1-silenced and control THP-1 cells (B) as well as TRAM KO and control THP-1 cells (C) infected with a DH5α strain at MOI 40. **(D and E)** Western blot analysis of pAkt (S473) and pIRF3 (S396) levels induced by *E. coli* particles in THP-1 WT and TRAM KO cells (D) as well as SLAMF1-silenced or control oligonucleotide–treated cells (E). Graphs (right) on Western blotting show quantification of protein levels relative to β-tubulin obtained with Odyssey software. **(F)** Western blot showing phospho-(S396) IRF3 and phospho-(S473) Akt levels in lysates of THP-1 cells coincubated with *E. coli* particles for 1 h in the presence or absence of TBK1-IKKε inhibitor (MRT67307), pan-Akt allosteric inhibitor (MK2206), or DMSO. Molecular weight is given in kilodaltons. **(G)** Bacterial killing assays by THP-1 cells with DMSO (<0.01%), 1 μM Akt inhibitor MK2206, or 2 μM TBK1-IKKε inhibitor MRT67307 upon infection by DH5α at MOI 40. Percent killing was calculated as 100 − (number of CFUs at time X/number of CFUs at time 0) × 100 for average values of technical replicates, and each dot on the graphs in B, C, and G represents a biological replicate from three independent experiments. Median values are shown by lines. Statistical significance was calculated by a Mann-Whitney nonparametric test. **, P < 0.01; ***, P < 0.001.

translational modifications of signaling molecules (Mogensen, 2009). We hypothesize that TLR4 signaling results in a shift from a Rab11 GDP-bound to a Rab11 GTP-bound active state. Moreover, previous research has demonstrated that FIPs prefer binding to GTP-bound Rab11 (Junutula et al., 2004). Thus, after the Rab11 GDP/GTP ratio shifts to the GTP-bound state, FIPs would connect cargo to Rab11 vesicles, which would enhance delivery of SLAMF1 and TRAM via class I FIPs from ERCs to *E. coli* phagosomes.

Mouse SLAMF1 was shown to be a bacterial sensor by itself, recognizing porins in the outer bacterial membrane (Berger et al., 2010). The regulatory role of mouse SLAMF1 upon TLR4 ligation by LPS is directly dependent on the porins present in crude LPS preparations or porins in the bacterial outer membrane (Berger et al., 2010). Unlike its mouse orthologue, human SLAMF1 did not require interaction with bacterial porins to elicit its effects on TLR4-mediated IFNβ production as similar data were obtained with both *E. coli* bioparticles and ultrapure LPS.

The delivery of TRAM to endosomes and phagosomes is crucial for the activation of the IRF3 signaling pathway and IFNβ induction (Kagan et al., 2008; Husebye et al., 2010). We found that SLAMF1 silencing caused a significant decrease in TRAM accumulation around *E. coli* phagosomes. Moreover, endogenous TRAM coimmunoprecipitated with SLAMF1. These data demonstrate that SLAMF1 is a critical regulator of TRAM recruitment to the phagosomes. We were able to map the domain in SLAMF1 involved in the interaction with TRAM to 15 C-terminal amino acids as both deletion of five C-terminal amino acids and substitution of amino acids at positions 321–324 abrogated interaction of SLAMF1 protein with TRAM. The interaction domain in TRAM was located outside the BB loop as TIR-TIR dimerization is not affected, and it was mapped to the N-terminal part of TRAM TIR domain between

aa 68–95. We found that mouse SLAMF1ct contains different amino acid sequences at positions corresponding with human 321–324 residues. This resulted in the absence of interaction between mouse SLAMF1 and TRAM, and consequently, LPS- or *E. coli*–induced IFNβ expression was not altered in *Slamf1*$^{-/-}$ BMDMs when compared with WT cells.

The failure to activate TBK1-IKKε kinase observed upon SLAMF1 silencing may affect the antibacterial functions of TBK1-IKKε (Radtke et al., 2007; Thurston et al., 2016). The Akt kinase, which is activated by TBK1-IKKε upon TLR4 ligation, is directly involved in the TLR4-mediated switch to glycolysis by phosphorylating crucial downstream target proteins (Krawczyk et al., 2010; Kelly and O'Neill, 2015). Moreover, Akt is involved in the activation of NADPH oxidase by the phosphorylating p47 subunit (Chen et al., 2003; Hoyal et al., 2003), which may result in ROS generation needed for bacterial killing (West et al., 2011). We demonstrate that SLAMF1 and TRAM were required for *E. coli*–mediated Akt phosphorylation via TBK1-IKKε as well as for the efficient bacterial killing. It is known that TLR2 and TLR4 ligands activate Akt S473 in a MyD88-dependent manner (Laird et al., 2009; Troutman et al., 2012). It should be noted that in contrast with these studies, we have used *E. coli* particles and found that Akt S473 phosphorylation was TRAM and SLAMF1 dependent. Akt phosphorylation induced by pure TLR2 and TLR4 ligands could be more dependent on MyD88, but it was not dependent on SLAMF1 or TRAM in THP-1 macrophages.

There is accumulating evidence on divergent regulation of TLR4 signaling and gene expression in different species (Schroder et al., 2012; Vaure and Liu, 2014). It is known that humans and old-world monkey species are highly sensitive to LPS with physiological changes induced by a dose at nanograms per kilogram, whereas rodents are highly insensitive to LPS with physiological changes only induced by a dose at milligrams per kilogram (Vaure and Liu, 2014). Many therapeutic agents that reduce inflammation and mortality in mouse septic shock models show no clinical benefit for humans (Poli-de-Figueiredo et al., 2008). Human monocyte-derived macrophages express much higher levels of *IFNβ* mRNA in response to LPS than mouse BMDM or thioglycolate-elicited peritoneal macrophages (Schroder et al., 2012). Our findings support higher LPS-induced secretion of IFNβ by human macrophages compared with BMDMs. Thus, during evolution, human macrophages must have acquired mechanisms to enhance TLR4-mediated IFNβ production in response to LPS or, vice versa, mouse cells developed less sensitive response to bacterial LPS. We suggest that SLAMF1-regulated transport of TRAM to the TLR4 signaling complex on bacterial phagosomes could be one of the features specific for human cells, which amplifies the IFNβ secretion. Thus, human SLAMF1 could potentially be targeted to regulate TLR4-mediated cytokine production in inflammatory conditions.

Materials and methods

Primary cells and cell lines

Use of human monocytes from blood donors was approved by the Regional Committees from Medical and Health Research Ethics at the Norwegian University of Science and Technology. Human monocytes were isolated from buffycoat by adherence as previously described (Husebye et al., 2010). In brief, freshly prepared buffycoat (St. Olavs Hospital) was diluted by 100 ml of PBS and applied on top of Lymphoprep (Axis-Shield) according to the manufacturer's instructions. PBMCs were collected and washed by HBSS (Sigma-Aldrich) four times with low-speed centrifugation (150–200 *g*). Cells were counted using Z2 Coulter particle count and size analyzer (Beckman Coulter) on program B, resuspended in RPMI 1640 (Sigma-Aldrich) supplemented with 5% of pooled human serum at a concentration of 8×10^6 per ml, and seeded to six-well (1 ml per well) or 24-well (0.5 ml per well) cell culture dishes. After a 45-min incubation allowing surface adherence of monocytes, the dishes were washed three times by HBSS to remove nonadherent cells. Monocytes were maintained in RPMI 1640 supplemented with 10% pooled human serum (St. Olavs Hospital) and used within 24 h after isolation. Monocyte-derived macrophages were obtained by differentiating cells for 8–10 d in RPMI 1640 with 10% human serum and 25 ng/ml rhM-CSF (216-MC-025; R&D Systems). THP-1 cells (ATCC) were cultured in RMPI 1640 supplemented by 10% heat-inactivated FCS, 100 nM penicillin/streptomycin (Thermo Fisher Scientific), and 5 µM β-mercaptoethanol (Sigma-Aldrich). THP-1 cells were differentiated with 50 ng/ml of PMA (Sigma-Aldrich) for 72 h, followed by 48 h in medium without PMA. HEK293T cells (ATCC) were cultured in DMEM with 10% FCS. For making the TRAM KO THP-1 cell line, LentiCRISPRv2 plasmid (a gift from F. Zhang; 52961; Addgene; Sanjana et al., 2014) was ligated with 5′-CACCGA TGACTTTGGTATCAAACC-3′ and 5′-AAACGGTTTGATACCAAA GTCATC-3′ for TRAM. Packaging plasmids pMD2.G and psPAX2 were used for producing lentivirus (provided by D. Trono, École Polytechnique Fédérale de Lausanne, Lausanne, Switzerland; 12260 and 12259; Addgene). HEK293T cells were cotransfected with the packaging and lentiCRISPRv2 plasmids and then washed after 16 h. The lentivirus-containing supernatants were collected after 48 h and used for transduction of THP-1 cells along with 8 µg/ml protamine sulphate. Transduced THP-1 cells were then selected with puromycin (1 µg/ml) for 1 mo and tested for TRAM protein expression by Western blotting. All cell lines were regularly checked for mycoplasma contamination.

Reagents and cell stimulation

pHrodo red *E. coli* and *S. aureus* as well as AF488-conjugated *E. coli* bioparticles were purchased from Thermo Fisher Scientific. Ultrapure 0111:B4, K12 LPS from *E. coli*, poly I:C, imidazoquinoline compound R848 (Resiquimod), thiazoloquinoline compound CL075, and synthetic diacylated lipoproteins FSL-1 (Pam2CGDPKHPKSF) and Pam3CSK4 (P3C) were from InvivoGen. Ultrapure K12 LPS or 0111:B4 LPS (InvivoGen) were used at concentrations of 100 ng/ml. *E. coli* bioparticles were reconstituted in 2 ml PBS, and 50 µl/well (1.5×10^7 particles) in 1 ml of media was used for cells in six-well plates (Nunc) or 35-mm glass-bottomed tissue cell dishes (MatTek Corporation), and 15 µl/well (0.45×10^7 particles) in 0.5 ml of media were used for 24-well plates (Nunc). The pan-Akt inhibitor MK2206 (1032350-13-2; Axon Medchem) and the TBK1-IKKε inhibitor MRT67307 (from P. Cohen, University of Dundee, Dundee, Scotland, UK; Clark et al., 2011) were diluted in DMSO at a concentration of 20 mM and stored at −80°C, and working solutions were prepared in cell culture media immediately before use.

Antibodies

The following primary antibodies were used: rabbit anti–TICAM-2/TRAM (GTX112785) from Genetex; rabbit mAb anti–human SLAMF1/SLAMF1 (10837-R008-50) from Sino Biological Inc.; mouse anti-GAPDH (ab9484) and rabbit anti–phospho-IRF3 Ser386 (ab76493) from Abcam; rabbit anti–phospho-Akt Ser473 (D9E; 4060), phospho-IRF3 Ser396 (4D4G; 4947), IkB-α (44D4; 4812), phospho–IkB-α (14D4; 2859), p38MAPK (9212), phospho-p38MAPK (Thr180/Tyr182; D3F9; 4511), TBK1/NAK (D1B4; 3504), phospho-TBK1/NAK (Ser172; D52C2; 5483), phospho-TAK1 (T184/187; 90C7; 4508), TAK1 5206, phospho–stress-activated protein kinase

(SAPK)/JNK (Thr183/Tyr185; 81E11; 4668), anti-DYKDDDDK tag (D6W5B)/Flag tag (14793), anti-MyD88 (D80F5; 4283), and phospho-STAT1 (Tyr701; D4A7; 7649) from Cell Signaling Technology; rabbit anti–total IRF3 (FL-425; sc-9082) and proliferating cell nuclear antigen (PCNA; FL-261; sc-7907) were from Santa Cruz Biotechnology, Inc.; Living Colors rabbit anti–full-length GFP polyclonal antibodies (632592) from Takara Bio Inc.; 4G10 platinum antiphosphotyrosine antibody biotin conjugated (16-452) from EMD Millipore; and mouse anti-GST antibodies (SAB4200237) and monoclonal mouse ANTI-FLAG M2 antibodies (F1804-200UG) from Sigma-Aldrich. Secondary antibodies (HRP linked) for Western blotting were swine anti–rabbit (P039901-2) and goat anti–mouse (P044701-2) from Dako/Agilent Technologies. The following antibodies were used for staining and/or IPs: rabbit anti-LAMP1 (ab24170) and GM130 antibody (EP892Y) cis-Golgi marker (ab52649) from Abcam; rabbit anti-EEA1 (H-300; sc-33585), TICAM2/TRAM (H-85), TLR4 (H-80; sc-10741), normal rabbit IgG (sc-2027), and normal mouse IgG (sc-2025) were from Santa Cruz Biotechnology, Inc.; rabbit anti-Rab11, low endotoxin, azide-free (LEAF)-purified mouse IgG1 isotype control (MOPC-21; 400124) and LEAF-purified mouse anti-CD150 (SLAMF1) A12 (7D4; 306310) were from BioLegend; and anti-SLAMF1 IgG1 (IPO-3) was provided by S.P. Sidorenko (Natural Academy of Sciences, Kiev, Ukraine; Sidorenko and Clark, 1993). Secondary antibodies for confocal microscopy were goat anti–mouse IgG (H+L) Alexa Fluor 405 conjugate (A-31553), Alexa Fluor 488 conjugate (A-11001), Alexa Fluor 647 conjugate (A-21235), goat anti–rabbit IgG (H+L) Alexa Fluor 405 conjugate (A-31556), Alexa Fluor 488 conjugate (A-11008), and DNA stain Hoechst 33342 (62249) from Thermo Fisher Scientific.

Imaging and image analysis

Confocal images were captured using either an LSM510 META (ZEISS) equipped with a Plan Apochromat 63× 1.4 NA oil immersion objective (images presented in Fig. 1 A and used for 3D modeling in Fig. 1 B) or a TCS SP8 (Leica Microsystems) equipped with a high-contrast Plan Apochromat 63× 1.40 NA oil CS2 objective. Fluorescence was captured by standard photomultiplier tube detectors (LSM 510 META; ZEISS), stimulated emission depletion hybrid detector, or photomultiplier tube detectors (TCS SP8). Acquisition software for the LSM 510 META was Zen microscope software (2012; ZEISS) and for the TCS SP8 was LAS AF software (4.0.0.11706; Leica Microsystems). Before imaging, cells were fixed with 2% paraformaldehyde in PBS on ice, and then immunostaining was performed as described previously (Husebye et al., 2010). In brief, upon fixation, the cells were permeabilized with PEM buffer (80 mM K-Pipes, pH 6.8, 5 mM EGTA, 1 mM $MgCl_2$, and 0.05% saponin) for 15 min on ice, quenched of free aldehyde groups in 50 mM NH_4Cl with 0.05% saponin for 5 min, and blocked in PBS with 20% human serum and 0.05% saponin. The cells were incubated with primary antibody in PBS with 2% human serum and 0.05% saponin overnight at 4°C or for 2 h at RT. Alexa Fluor–labeled secondary antibodies (Invitrogen/Thermo Fisher Scientific) were incubated for 15 min at RT after three washes in PBS with 0.05% saponin. If double staining was made, cells were sequentially stained by primary antibodies, specific secondary Alexa Fluor–conjugated antibodies, second primary antibodies, and then specific secondary Alexa Fluor–conjugated antibodies. Images of stained cells, washed in PBS with 0.05% saponin and left in PBS, were captured at RT. 3D data were captured with identical settings, which were also adjusted to avoid saturation of voxel (3D pixels) intensities. For colocalization analysis, the Coloc 2 plugin with thresholds in Fiji (ImageJ; National Institutes of Health) application was applied (Schindelin et al., 2012). The pHrodo fluorescence was used to spot or surface render the volume of individual phagosomes when *E. coli* pHrodo, *S. aureus* pHrodo red, or AF488-conjugated *E. coli* particles were used. A binary mask was created around bacterial particles (Process/Make Binary function) and used to define the regions for quantification of MIs for TRAM and SLAMF1 voxels in original images and to quantify *E. coli* pHrodo particles MI when redirected to the original image. *E. coli* pHrodo MI was evaluated to quantify acidification of *E. coli*–containing phagosomes in cells treated by control or *SLAMF1* siRNA. For analysis of the sum of voxel intensities of SLAMF1 inside Golgi rings, GM130 staining was used to define the region to evaluate SLAMF1 intensities for individual 3D Golgi ring structure. Using ImageJ/Fiji software, 3D Golgi ring structures were selected as a region of interest (ROI) and used as a mask to obtain a numerical value of the relative amount of SLAMF1 as a sum of voxel intensities for SLAMF1 staining in Golgi ring ROIs from original image. ImarisXT software (Bitplane) was used to surface render the imaged GM130-positive structures, giving one surface for each. The values for voxel intensities did not follow a Gaussian distribution, and therefore we used median as a measure of average intensities and the nonparametric Mann-Whitney test to evaluate statistical significance in Prism (5.03; GraphPad Software).

siRNA treatment

Oligonucleotides used for silencing were AllStars negative control siRNA (SI03650318), FlexiTube siRNA Hs_SLAMF1_2 (SI00047250), Hs_MYD88_2 (SI00038297), Hs_TICAM2_2 (SI00130893), Hs_RAB11A_5 (SI00301553), and Hs_RAB11B_6 (SI02662695; QIAGEN). On day 7, cells were transfected by silencing oligonucleotides (20 nM final concentration) using Lipofectamine 3000 (L3000008) from Invitrogen/Thermo Fisher Scientific as suggested by the manufacturer. Cells were stimulated by LPS or *E. coli* particles 96 h after transfection. For THP-1 cells, cells were seeded in six-well plates (Nunc) 0.4×10^6 per well in antibiotic-free media supplemented by 40 ng/ml of PMA. Transfection of siRNA was performed for 24 h, media was changed to PMA-free for 72 h, and cells were kept for another 48 h before stimulation by LPS or *E. coli* particles.

Quantitative PCR (qPCR)

Total RNA was isolated form the cells using Qiazol reagent (79306; QIAGEN), and chloroform extraction followed by purification was performed on RNeasy Mini columns with DNase digestion step (QIAGEN). cDNA was prepared with the Maxima first strand cDNA synthesis kit for RT-qPCR (Thermo Fisher Scientific) according to the manufacturer's protocol. qPCR was performed using the PerfeCTa qPCR FastMix (Quanta Biosciences) in replicates and was cycled in a StepOnePlus real-time PCR cycler. The following TaqMan gene expression assays (Applied Biosystems) were used: *IFNβ* (Hs01077958_s1), *TNF* (Hs00174128_m1), *SLAMF1* (Hs00900288_m1), *TBP* (Hs00427620_m1), *CXCL10* (Hs01124251_g1), *Rab11a* (Hs00366449_g1), and *Rab11b* (Hs00188448_m1) for human cells; and *Ifnβ* (Mm00439552_s1), *Tnf* (Mm00443258_m1), and *Tbp* (Mm01277042_m1) for mouse cells. No–reverse transcription controls were negative. The level of *TBP* mRNA was used for normalization, and results are presented as relative expression compared with the control untreated sample. Relative expression was calculated using the Pfaffl's mathematical model (Pfaffl, 2001). Results are presented as means and SD of expression fold change for biological replicates relative to nonstimulated cells. Statistical significance was evaluated with Prism software. Data distribution was assumed to be normal, but this was not formally tested. The difference between the two groups was determined by the two-tailed *t* test.

Cloning, expression vectors, and DNA transfection

Phusion high-fidelity DNA polymerase and respective Fast Digest enzymes (Thermo Fisher Scientific) were used for cDNA recloning.

Plasmids we purified by the Endofree plasmid maxi kit (QIAGEN). Sequencing of plasmids was done at the Eurofins genomics facility. Primers for cloning are listed below. *SLAMF1* coding sequence was subcloned from retroviral vector (from A. Taranin, Siberian Branch of the Russian Academy of Sciences, Novosibirsk, Russia) to pcDNA3.1 (Invitrogen), C-terminal DYKDDDDK (Flag tag) vector (Takara Bio Inc.), deletion mutants of SLAMF1 made in pcDNA3.1 vector, or C-terminal DYK DDDDK vector. Human $TRIF^{HA}$ and $TRAM^{YFP}$ from K. Fitzgerald (University of Massachusetts Medical School, Worcester, MA) were used for transfections or as templates for subcloning and making TRAM deletion mutants. $Rab11a^{Flag}$ coding construct was described previously (Klein et al., 2015); Rab11FIP1, Rab11FIP2 ΔC2, Rab11FIP2, Rab11FIP3, Rab11FIP4, and Rab11FIP5 in pEGFPC1 vector were from M. McCaffrey (University College Cork, Cork, Ireland). Rab11aQ70L and Rab11aS25N were PCR amplified from pEGFP-Rab11Q70L and pEGFP-Rab11aS25N (Husebye et al., 2010), respectively. The amplified fragments were inserted into SalI- and BamHI-restricted pECFP-C1 vector. TLR4 was subcloned from a $TLR4^{Cherry}$ construct (Husebye et al., 2010) to a C-terminal DYKDDDDK vector. Mouse SLAMF1 was subcloned to a C-terminal DYKDDDDK vector, and mouse TRAM was subcloned from a GeneScript ORF clone (OMu22478D) to pEGFP-N1 vector (Takara Bio Inc.). pDUO-hMD-2/CD14 (Invivogen) was coexpressed with TLR4 to ensure TLR4 dimer formation. HEK 293T cells in six-well plates were transfected by 0.2–0.4 µg of vector/well using Genejuice transfection reagent (EMD Millipore). Lysates were prepared 48 h after transfection. Primers used for cloning are listed in Table 1.

IPs

HEK293T cells expressing Flag-tagged proteins or macrophages for endogenous IPs were lysed using 1× lysis buffer (150 mM NaCl, 50 mM Tris-HCl, pH 8.0, 1 mM EDTA, and 1% NP-40) or 1× lysis buffer with high salt (400 mM NaCl, 50 mM Tris-HCl, pH 7.5, 1% Triton X-100, and 5 mM EDTA) for antiphosphotyrosine IPs supplemented with EDTA-free Complete mini protease inhibitor cocktail tablets and PhosSTOP phosphatase inhibitor cocktail (Roche), 50 mM NaF, and 2 mM Na_3VO_3 (Sigma-Aldrich). IPs were carried out by rotation at 4°C for 2 h of cell lysates with either anti-Flag (M2) agarose (Sigma-Aldrich) or specific antibodies coupled to Dynabeads (M-270 Epoxy; Thermo Fisher Scientific) or phosphotyrosine-biotinylated antibodies on streptavidin beads (Invitrogen). Agarose, Sepharose, or Dynabeads were washed five times by respective lysis buffers and heated for 5 min with 1× NuPAGE LDS sample buffer (Thermo Fisher Scientific) for agarose and Sepharose beads or eluted by elution buffer (from Dynabeads co-IP kit; 14321D; Thermo Fisher Scientific) for Dynabeads before analysis by Western blotting.

Western blotting

Cell lysates other than those used as controls in IPs were prepared by simultaneous extraction of proteins and total RNA using Qiazol reagent as suggested by the manufacturer. Protein pellets were dissolved by heating protein pellets for 10 min at 95°C in buffer containing 4 M urea, 1% SDS (Sigma-Aldrich), and NuPAGE LDS sample buffer (4×; Thermo Fisher Scientific). Otherwise, lysates were made using 1× RIPA lysis buffer (150 mM NaCl, 50 mM Tris-HCl, pH 7.5, 1% Triton X-100, 5 mM EDTA, protease inhibitors, and phosphatase inhibitors). For Western blot analysis, we used precast protein gels NuPAGE, Novex, iBlot transfer stacks, and the iBlot gel transfer device (Thermo Fisher Scientific).

Lentiviral transduction

For making the TRAM KO cell line, LentiCRISPRv2 plasmid (gift from F. Zhang; 52961; Addgene; Sanjana et al., 2014) was ligated with 5′-CACCGATGACTTTGGTATCAAACC-3′ and 5′-AAA CGGTTTGATACCAAAGTCATC-3′ for TRAM. The second-generation packaging plasmids pMD2.G and psPAX2 were used for producing lentivirus (provided by D. Trono; 12260 and 12259; Addgene). HEK293T cells were cotransfected with the packaging and lentiCRISPRv2 plasmids and then washed after 16 h. The lentivirus-containing supernatants were collected after 48 h and used for transduction of THP-1 WT cells along with protamine sulphate (8 µg/ml final concentration). Transduced THP-1 cells were selected with puromycin (1 µg/ml) for 1 mo and then tested for TRAM protein expression by Western blotting. Lentivirus construct of SLAMF1 was prepared by cloning full-size SLAMF1 with or without Flag tag to the bicistronic lentiviral expression vector pLVX-EF1α-IRES-ZsGreen1 (Takara Bio Inc.; primers are listed in Table 1). The construct was sequenced and cotransfected with packaging plasmids (psPAX2 and pMD2.G provided by D. Trono; 12260 and 12259; Addgene) to produce pseudoviral particles in HEK293T cells. Supernatants were collected at 48 and 72 h, combined, and concentrated using Lenti-X concentrator (631231; Takara Bio Inc.). Viral particles were titrated in HEK293T cells. Titrated virus particles, which gave 90–100% of transduction efficiencies, were subsequently used for transduction of primary human macrophages (resulting in 30–40% of ZsGreen-positive cells). Macrophages were infected on day 6 of differentiation, media was changed after 24 h, and stimulation by LPS (100 ng/ml) was performed 72 h after transduction. Cell lysates for simultaneous RNA/protein isolation were prepared using Qiazol reagent.

Flow cytometry

Untreated or LPS-stimulated monocyte-derived macrophages were detached using accutase (A6964; Sigma-Aldrich) and stained with a cocktail of antibodies against human CD14 (MΦP9) FITC conjugated from BD and SLAMF1 IgG1 (IPO-3) mAbs labeled by AF647 using the Alexa Fluor 647 protein labeling kit (A20173) for 30 min on ice. Flow cytometry was performed using LSR II (BD) with FACS Diva software (BD). Samples were analyzed with FlowJo software (7.6; TreeStar).

ELISA and multiplex cytokine assay

TNF in supernatants was detected using a human TNF-α DuoSet ELISA (DY210-05; R&D Systems), and IFNβ level was detected using VeriKine-HS human IFNβ serum ELISA kit (41415; PBL Assay Science). Supernatants were also analyzed by multiplex cytokine assay (Bio-Plex; Bio-Rad Laboratories) for IL-1β, IL-6, IL-8, and CXCL-10/IP-10. TNF in BMDM supernatants was detected using mouse TNF-α DuoSet ELISA (DY410-05; R&D Systems), and IFNβ level was assessed using a VeriKine-HS mouse IFNβ serum ELISA kit (42410-1; PBL Assay Science). Results are presented as means and SD for biological replicates for representative donors (primary human macrophages) or at least three independent experiments for model cell line THP-1. Statistical significance was evaluated in Prism software. Data distribution was assumed to be normal, but this was not formally tested. The difference between the two groups was determined by a two-tailed *t* test.

Blocking IFN receptors by specific antibodies

Differentiated THP-1 cells in six-well plates were incubated for 30 min at 37°C with 2.5 µg/ml anti-IFNAR chain 2 antibodies, clone MMH AR-2 isotype IgG2a (MAB1155; EMD Millipore), or control mAbs LEAF-purified mouse IgG2a κ isotype MOPC-173 (400224; BioLegend). After preincubation with mAbs, cells were stimulated with LPS (100 ng/ml) and lysed using Qiazol reagent for simultaneous extraction of proteins and total RNA.

Table 1. **Primers used for cloning of full-size or deletion mutants of SLAMF1, TRAM, TLR4, and Rab11 FIP2.**

Construct	For/Rev	Primer sequence (5′–3′)	Restriction enzyme	PCR product mapped on nucleotide sequence
SLAMF1 (NM_003037.3)				
pcDNA3.1 and pLVX-EF1α-IRES-ZsGreen1	For	TTCGAATTCTGATGGGATCCCAAGGGGCTCC	EcoRI	367–1,374
	Rev	GCAGCGGCCGCTCAGCTCTCTGGAAGTGTCA	NotI	
C-terminal DYKDDDDK	For	TTAGAATTCATGGATCCCAAGGGGCTCC	EcoRI	367–1,371
	Rev	GGTACCTCGAGAGCTCTCTGGAAGTGTCACAC	XhoI	
pGEX-2TK	For	TATGGATCCCAGTTGAGAAGAAGAGGTAAAACG	BamHI	1,141–1,374
	Rev	ATAGAATTCTCAGCTCTCTGGAAGTGTCAC	EcoRI	
SLAMF1 (NM_003037.3) deletion mutants to C-terminal DYKDDDDK				
All deletion mutants	For	TTAGAATTCATGGATCCCAAGGGGCTCC	EcoRI	N/a
1–265 aa	Rev	GGTACCTCGAGATTTACCTCTTCTTCTCAACTGTAG	XhoI	367–1,161
1–326 aa	Rev	GTACCTCGAGAGACTGTGATGGAATTTGTTTCCTG	XhoI	367–1,344
1–330 aa	Rev	GTACCTCGAGACACACTAGCATAGACTGTGATG	XhoI	367–1,356
SLAMF1 (NM_003037.3) deletion mutant to pcDNA3.1				
1–265 aa	For	TTCGAATTCTGATGGGATCCCAAGGGGCTCC	EcoRI	367–1,161
	Rev	TTAAGCGGCCGCTCATTTACCTCTTCTTCTCAACTG	NotI	
SLAMF1 (NM_003037.3) mutants with amino acid substitutions to C-terminal DYKDDDDK				
SLAMF1 Y281F	For	TTAGAATTCATGGATCCCAAGGGGCTCC	EcoRI	367–1,225
	Rev	GTTTCTGGACTTGGGCAAAGATCGTAAGGC		
	For	GCCTTACGATCTTTGCCCAAGTCCAGAAAC		1,196–1,371
	Rev	GGTACCTCGAGATTTACCTCTTCTTCTCAACTGTAG	XhoI	
SLAMF1 Y327F	For	TTAGAATTCATGGATCCCAAGGGGCTCC	EcoRI	367–1,371
	Rev	GGTACCTCGAGAGCTCTCTGGAAGTGTCACACTAGCAAAGAC TGTG	XhoI	
SLAMF1 TNSI/PNPT	For	TTAGAATTCATGGATCCCAAGGGGCTCC	EcoRI	367–1,341
	Rev	TGTGGTGGGGTTTGGTTCCTGGACAGACTCTGG		
	For	GAACCAAACCCCACCACAGTCTATGCTAGTGTGACACTTC		1,324–1,371[a]
	Rev[b]	CTTGTCATCGTCGTCCTTG		
TRAM/TICAM-2 (NM_021649.7)				
C-terminal DYKDDDDK	For	CATGAATTCATGGGTATCGGGAAGTCTAAA	EcoRI	443–1,147
	Rev	TTAACTCGAGCGGCAATAAATTGTCTTTGTACC	XhoI	
TRAM deletion mutants to C-terminal DYKDDDDK				
1–68 aa	For	CATGAATTCATGGGTATCGGGAAGTCTAAA	EcoRI	443–646
	Rev	TTAACTCGAGCCATCTCTTCCACGCTCTGAGC	XhoI	
1–79 aa	For	CATGAATTCATGGGTATCGGGAAGTCTAAA	EcoRI	443–679
	Rev	TTACCTCGAGAGAGGAACACCTCTTCTTCAGC	XhoI	
1–90 aa	For	CATGAATTCATGGGTATCGGGAAGTCTAAA	EcoRI	443–712
	Rev	TTACCTCGAGATGTGTCATCTTCTGCATGCAATATC	XhoI	
1–100 aa	For	CATGAATTCATGGGTATCGGGAAGTCTAAA	EcoRI	443–742
	Rev	TTACCTCGAGATAGCAGATTCTGGACTCTGAGG	XhoI	
1–120 aa	For	CATGAATTCATGGGTATCGGGAAGTCTAAA	EcoRI	443–802
	Rev	TTACCTCGAGACTGTCTGCCACATGGCATCTC	XhoI	
68–235 aa	For	CATGAATTCATGTTTGAAGAAGAAGCTGAA	EcoRI	644–1,147
	Rev	TTAACTCGAGCGGCAATAAATTGTCTTTGTACC	XhoI	
68–176 aa	For	CATGAATTCATGTTTGAAGAAGAAGCTGAA	EcoRI	644–970
	Rev	TTAACTCGAGCCAGGGGCCGCATGGGTATAACAG	XhoI	
158–235 aa	For	CATGAATTCATGAACTCCGTTAACAGGCAGC	EcoRI	914–1,147
	Rev	TTAACTCGAGCGGCAATAAATTGTCTTTGTACC	XhoI	
TLR4 (NM_138554.4)				
C-terminal DYKDDDDK	For	CGGTCGACCGAGATCTCATGATGTCTGCCTCGCGCCTGG	N/a	299–2,815
	Rev	CTTGTAGTCGCCGGTACCGATAGATGTTGCTTCCTGCCAATTG	N/a	
***Mus Musculus* TRAM/Ticam-2 (NM_173394.3) to EGFP-N1**				
1–232 aa	For	ACTAAGCTTATGGGTGTTGGGAAGTCTAAAC	HindIII	477–1,175
	Rev	ATATGGATCCCGGGCAATGAACTGTTTCTGCGAC	BamHI	

Table 1. **Primers used for cloning of full-size or deletion mutants of SLAMF1, TRAM, TLR4, and Rab11 FIP2.** *(Continued)*

Construct	For/Rev	Primer sequence (5′–3′)	Restriction enzyme	PCR product mapped on nucleotide sequence
***M. Musculus* Slamf1 (NM_013730.4) from pDisplay vector to C-terminal DYKDDDDK**				
30–343 aa	For	TTGGAATTCGGCTTGGGGATATCCACCATGG	EcoRI	183–1,127
	Rev	TATACCTCGAGAGCTCTCTGGCAGTGTCACACTG	XhoI	
Rab11 FIP2 (NM_014904.2) and deletion mutants to N-terminal DYK DDDDK				
All constructs	For	GCCCGAATTCGGCTGTCCGAGCAAGCCCAAAAG	EcoRI	
1–512 aa	Rev	ATAGCGGCCGCTCATTAACTGTTAGAGAATTTGCCAGC	NotI	446–1,980
1–327 aa	Rev	ATAGCGGCCGCTCATTCGCTGCTTTCTTCAAATGG	NotI	446–1,429
1–290 aa	Rev	ATAGCGGCCGCTTACACAATGCTGTCAGGTTGG	NotI	446–1,310
1–254 aa	Rev	ATAGCGGCCGCTTATCCGAGAAGATGTGTTTGACC	NotI	446–1,199
1–192 aa	Rev	ATAGCGGCCGCTTAGTGAGTACTTGGAATGATTGC	NotI	446–1,016
Rab11a (NM_004663.4) QL and SN mutants to pECFP-C1				
1–216 aa	For	ATCAGTCGACATGGGCACCCGCGACGAC	SalI	128–145
	Rev	TTAAGGATCCTTATATGTTCTGACAGCACTG	BamHI	758–774

For, forward; QL, Rab11a Q70L mutant; Rev, reverse; SN, Rab11a S25N mutant.
[a]Partially on vector sequence.
[b]On C-terminal DYKDDDDK vector.

GST pulldown assays

The GST fusion protein construct of SLAMF1ct (GST-SLAMF1ct) was prepared by cloning SLAMF1ct (corresponding with 259–335 aa of SLAMF1 protein; UniProtKB, Q13291) to pGEX-2TK vector (GE Healthcare) with the help of V. Kashuba (Karolinska Institute, Stockholm, Sweden). The sequenced plasmid was transformed into the BL21 DE3 bacterial strain (New England Biolabs, Inc.) or to the TKX1 strain (Agilent Technologies) for production of tyrosine-phosphorylated GST-SLAMF1ct-antiphosphotyrosine. Expression and purification of GST fusion proteins were performed as described previously (Shlapatska et al., 2001). For protein purification and pulldown assays, we used Glutathione high-capacity magnetic agarose beads (G0924; Sigma-Aldrich). Cell lysates of untreated and LPS-stimulated macrophages were prepared in 1× lysis buffer (0.5% NP-40, 150 mM NaCl, and 50 mM Tris-HCl, pH 8.0). Pulldowns were performed as described previously (Shlapatska et al., 2001).

Mouse BMDM differentiation and stimulation

All protocols on animal work were approved by the Norwegian National Animal Research Authorities and were carried out in accordance with Norwegian and European regulations and guidelines. BMDM cultures were generated from bone marrow aspirates extracted from the femurs of C57BL/6 8–10-wk-old male control mice or from *Slamf1*$^{-/-}$ C57BL/6 mice (Wang et al., 2004). Cells were cultured in complete RPMI 1640 medium containing 20% of L929-conditioned media produced in-house for 8–10 d in sterile Petri dishes; cells were counted and seeded to 24-well cell culture plates in RPMI 1640 with 10% FCS at concentrations of 0.3×10^6 per well in triplicate, left overnight, and treated the next day in fresh media by 100 ng/ml ultrapure LPS (Invivogen) or 50 µg/well for six-well plates or 20 µg/well for 24-well plates of *E. coli* particles. Cell lysates for RNA isolation were made using Qiazol reagent.

ROS activation assay

Primary human macrophages (in six-well plates) were treated by siRNA as described in the siRNA treatment section, and treated by *E. coli* red pHrodo bacterial particles (excitation wavelength, 561 nm) in 0.5 ml RPMI 1640 containing 10% human serum on water bath (for 20 min incubation) or in a CO_2 incubator (for 120 min incubation). Freshly dissolved in washing buffer (reagent A) or dihydrorhodamine 123 (DHR-123; excitation wavelength, 488 nm; reagent E), both from the PHAGOBURST kit (Glycotope Biotechnology), was added to the wells (except for control well, to which washing buffer was added) for the last 10 min of incubation. After stimulation, cells were placed on ice, washed by cold PBS, incubated with accutase (Sigma-Aldrich) on ice for 5 min, and scraped using cell scrapers. Cells were washed by flow wash (PBS with 0.5% FCS), fixed by fixation buffer (BD), washed by PBS, and analyzed by flow cytometry using LSR II with FACS Diva software. In FlowJo software, cells were gated for pHrodo-positive cells, and DHR-123 fluorescence was presented on the graphs for this gate.

Bacterial killing assay

THP-1 cells were plated at 2×10^5 cells/well in 24-well plates and differentiated as described in the Primary cells and cell lines section for 5 d. Cells were washed and transferred to serum-free RPMI medium. Live DH5α *E. coli* were added at an MOI of 40. *E. coli* were centrifuged onto differentiated THP-1 monolayers at 2,000 rpm for 5 min at 4°C. Plates were warmed to 37°C for 15 min in a water bath. Each well was then washed 3× with ice-cold PBS and incubated with warm 10% FCS RPMI medium containing 100 µg/ml of gentamycin for 30 min at 37°C to remove extracellular bacteria. If inhibitors were used in the assay, either DMSO or inhibitors were added to the media at designated concentrations. Cells were washed again 2× with PBS. This time point (45 min after adding bacteria) was designated as time 0. To measure colony-forming units (CFUs) at the end of incubation time, triplicate wells were washed and lysed in 1 ml sterile water. Plates for time points 1 h and 1.5 h were further incubated at 37°C in a CO_2 incubator in medium with 10% FCS without antibiotics and with or without kinase inhibitors. At each time point, triplicate wells were washed 3× with PBS before lysing the cells. Viable counts were determined by plating 10 µl of 10-fold dilutions, 1:100 and 1:1,000, onto Luria-Bertani agar (in triplicates to account for technical pipetting error). CFUs were counted at each time point including time 0. Percent killing was calculated as 100 − (number of CFUs at time X/number of CFUs at time 0) × 100 for average values

of technical replicates. Statistical significance was calculated in Prism software for biological replicates using unpaired two-tailed tests.

Online supplemental material

Fig. S1 shows that LPS treatment induces SLAMF1 expression in human cells, resulting in its surface localization, and that the increase in SLAMF1 expression is not dependent on signaling from IFNAR. Fig. S2 shows that SLAMF1 is involved in regulation of *E. coli*– or LPS-mediated but not TLR3-, TLR8-, or RIG-I/MDA5-mediated *IFNβ* or *TNF* mRNA expression. Fig. S3 shows that knockdown of SLAMF1 in THP-1 cells impairs TLR4-mediated phosphorylation of TBK1, IRF3, and TAK1 in response to LPS or *E. coli* particles. Fig. S4 shows that SLAMF1 relocalizes from ERCs to early and late *E. coli* phagosomes but not to *S. aureus* phagosomes and that SLAMF1 is required for *E. coli* phagosome acidification in human cells. Fig. S5 shows that SLAMF1 interaction with TRAM is independent from SLAMF1 tyrosine phosphorylation. Fig. S6 shows that TLR4-mediated *IFNβ* and *TNF* mRNA expression and corresponding cytokine secretion are not altered in *Slamf1*$^{-/-}$ BMDMs and provides human and murine SLAMF1 and TRAM proteins sequence alignments. Fig. S7 shows that *E. coli*–mediated Akt phosphorylation in human macrophages is not dependent on MyD88 expression and that TLR2- and TLR4-induced phosphorylation of Akt is weak and not much dependent on *SLAMF1* or *TRAM* expression.

Acknowledgments

We thank S. Sidorenko, V. Kashuba, and M. McCaffrey for providing reagents and V. Boyartchuk for expert advice. Confocal imaging was performed at the Cellular and Molecular Imaging Core Facility of the Norwegian University of Science and Technology.

This work was supported by the Research Council of Norway through its Centers of Excellence funding scheme grant 223255/F50 (to T. Espevik), by the Norwegian University of Science and Technology's Onsager Fellowship (to R.K. Kandasamy), by grants from the Liaison Committee for Education, Research and Innovation in Central Norway (to T. Espevik), and by the Joint Research Committee between St. Olavs Hospital and Faculty of Medicine and Health Science of the Norwegian University of Science and Technology (to H. Husebye).

The authors declare no competing financial interests.

Author contributions: Conceptualization: M. Yurchenko, H. Husebye, and T. Espevik; Methodology: M. Yurchenko, H. Husebye, A. Skjesol, and T. Espevik; Investigation: M. Yurchenko, A. Skjesol, L. Ryan, H. Husebye, G.M. Richard, and N. Wang; Writing, original draft: M. Yurchenko; Writing, review and editing: M. Yurchenko, A. Skjesol, H. Husebye, C. Terhost, and T. Espevik; Supervision: H. Husebye and T. Espevik; Resources: R.K. Kandasamy, C. Terhorst, and N. Wang.

Submitted: 6 July 2017
Revised: 31 October 2017
Accepted: 20 December 2017

References

Avota, E., E. Gulbins, and S. Schneider-Schaulies. 2011. DC-SIGN mediated sphingomyelinase-activation and ceramide generation is essential for enhancement of viral uptake in dendritic cells. *PLoS Pathog.* 7:e1001290. https://doi.org/10.1371/journal.ppat.1001290

Berger, S.B., X. Romero, C. Ma, G. Wang, W.A. Faubion, G. Liao, E. Compeer, M. Keszei, L. Rameh, N. Wang, et al. 2010. SLAM is a microbial sensor that regulates bacterial phagosome functions in macrophages. *Nat. Immunol.* 11:920–927. https://doi.org/10.1038/ni.1931

Chang, L., and M. Karin. 2001. Mammalian MAP kinase signalling cascades. *Nature.* 410:37–40. https://doi.org/10.1038/35065000

Chen, Q., D.W. Powell, M.J. Rane, S. Singh, W. Butt, J.B. Klein, and K.R. McLeish. 2003. Akt phosphorylates p47phox and mediates respiratory burst activity in human neutrophils. *J. Immunol.* 170:5302–5308. https://doi.org/10.4049/jimmunol.170.10.5302

Clark, K., M. Peggie, L. Plater, R.J. Sorcek, E.R. Young, J.B. Madwed, J. Hough, E.G. McIver, and P. Cohen. 2011. Novel cross-talk within the IKK family controls innate immunity. *Biochem. J.* 434:93–104. https://doi.org/10.1042/BJ20101701

Cocks, B.G., C.C. Chang, J.M. Carballido, H. Yssel, J.E. de Vries, and G. Aversa. 1995. A novel receptor involved in T-cell activation. *Nature.* 376:260–263. https://doi.org/10.1038/376260a0

Everts, B., E. Amiel, S.C. Huang, A.M. Smith, C.H. Chang, W.Y. Lam, V. Redmann, T.C. Freitas, J. Blagih, G.J. van der Windt, et al. 2014. TLR-driven early glycolytic reprogramming via the kinases TBK1-IKKε supports the anabolic demands of dendritic cell activation. *Nat. Immunol.* 15:323–332. https://doi.org/10.1038/ni.2833

Farina, C., D. Theil, B. Semlinger, R. Hohlfeld, and E. Meinl. 2004. Distinct responses of monocytes to Toll-like receptor ligands and inflammatory cytokines. *Int. Immunol.* 16:799–809. https://doi.org/10.1093/intimm/dxh083

Fitzgerald, K.A., S.M. McWhirter, K.L. Faia, D.C. Rowe, E. Latz, D.T. Golenbock, A.J. Coyle, S.M. Liao, and T. Maniatis. 2003a. IKKepsilon and TBK1 are essential components of the IRF3 signaling pathway. *Nat. Immunol.* 4:491–496. https://doi.org/10.1038/ni921

Fitzgerald, K.A., D.C. Rowe, B.J. Barnes, D.R. Caffrey, A. Visintin, E. Latz, B. Monks, P.M. Pitha, and D.T. Golenbock. 2003b. LPS-TLR4 signaling to IRF-3/7 and NF-kappaB involves the toll adapters TRAM and TRIF. *J. Exp. Med.* 198:1043–1055. https://doi.org/10.1084/jem.20031023

Fitzgerald, K.A., D.C. Rowe, and D.T. Golenbock. 2004. Endotoxin recognition and signal transduction by the TLR4/MD2-complex. *Microbes Infect.* 6:1361–1367. https://doi.org/10.1016/j.micinf.2004.08.015

Ford, E., and D. Thanos. 2010. The transcriptional code of human IFN-beta gene expression. *Biochim. Biophys. Acta.* 1799:328–336. https://doi.org/10.1016/j.bbagrm.2010.01.010

Gidon, A., S. Bardin, B. Cinquin, J. Boulanger, F. Waharte, L. Heliot, H. de la Salle, D. Hanau, C. Kervrann, B. Goud, and J. Salamero. 2012. A Rab11A/myosin Vb/Rab11-FIP2 complex frames two late recycling steps of langerin from the ERC to the plasma membrane. *Traffic.* 13:815–833. https://doi.org/10.1111/j.1600-0854.2012.01354.x

Guichard, A., V. Nizet, and E. Bier. 2014. RAB11-mediated trafficking in host-pathogen interactions. *Nat. Rev. Microbiol.* 12:624–634. https://doi.org/10.1038/nrmicro3325

Horgan, C.P., and M.W. McCaffrey. 2009. The dynamic Rab11-FIPs. *Biochem. Soc. Trans.* 37:1032–1036. https://doi.org/10.1042/BST0371032

Hoyal, C.R., A. Gutierrez, B.M. Young, S.D. Catz, J.H. Lin, P.N. Tsichlis, and B.M. Babior. 2003. Modulation of p47PHOX activity by site-specific phosphorylation: Akt-dependent activation of the NADPH oxidase. *Proc. Natl. Acad. Sci. USA.* 100:5130–5135. https://doi.org/10.1073/pnas.1031526100

Husebye, H., Ø. Halaas, H. Stenmark, G. Tunheim, Ø. Sandanger, B. Bogen, A. Brech, E. Latz, and T. Espevik. 2006. Endocytic pathways regulate Toll-like receptor 4 signaling and link innate and adaptive immunity. *EMBO J.* 25:683–692. https://doi.org/10.1038/sj.emboj.7600991

Husebye, H., M.H. Aune, J. Stenvik, E. Samstad, F. Skjeldal, O. Halaas, N.J. Nilsen, H. Stenmark, E. Latz, E. Lien, et al. 2010. The Rab11a GTPase controls Toll-like receptor 4-induced activation of interferon regulatory factor-3 on phagosomes. *Immunity.* 33:583–596. https://doi.org/10.1016/j.immuni.2010.09.010

Junutula, J.R., E. Schonteich, G.M. Wilson, A.A. Peden, R.H. Scheller, and R. Prekeris. 2004. Molecular characterization of Rab11 interactions with members of the family of Rab11-interacting proteins. *J. Biol. Chem.* 279:33430–33437. https://doi.org/10.1074/jbc.M404633200

Kagan, J.C., T. Su, T. Horng, A. Chow, S. Akira, and R. Medzhitov. 2008. TRAM couples endocytosis of Toll-like receptor 4 to the induction of interferon-beta. *Nat. Immunol.* 9:361–368. https://doi.org/10.1038/ni1569

Kelly, B., and L.A. O'Neill. 2015. Metabolic reprogramming in macrophages and dendritic cells in innate immunity. *Cell Res.* 25:771–784. https://doi.org/10.1038/cr.2015.68

Klein, D.C., A. Skjesol, E.D. Kers-Rebel, T. Sherstova, B. Sporsheim, K.W. Egeberg, B.T. Stokke, T. Espevik, and H. Husebye. 2015. CD14, TLR4 and TRAM Show Different Trafficking Dynamics During LPS Stimulation. *Traffic.* 16:677–690. https://doi.org/10.1111/tra.12274

Krawczyk, C.M., T. Holowka, J. Sun, J. Blagih, E. Amiel, R.J. DeBerardinis, J.R. Cross, E. Jung, C.B. Thompson, R.G. Jones, and E.J. Pearce. 2010. Toll-like receptor-induced changes in glycolytic metabolism regulate

dendritic cell activation. *Blood.* 115:4742–4749. https://doi.org/10.1182/blood-2009-10-249540

Laird, M.H., S.H. Rhee, D.J. Perkins, A.E. Medvedev, W. Piao, M.J. Fenton, and S.N. Vogel. 2009. TLR4/MyD88/PI3K interactions regulate TLR4 signaling. *J. Leukoc. Biol.* 85:966–977. https://doi.org/10.1189/jlb.1208763

Lindsay, A.J., and M.W. McCaffrey. 2004. The C2 domains of the class I Rab11 family of interacting proteins target recycling vesicles to the plasma membrane. *J. Cell Sci.* 117:4365–4375. https://doi.org/10.1242/jcs.01280

Ma, C., N. Wang, C. Detre, G. Wang, M. O'Keeffe, and C. Terhorst. 2012. Receptor signaling lymphocyte-activation molecule family 1 (Slamf1) regulates membrane fusion and NADPH oxidase 2 (NOX2) activity by recruiting a Beclin-1/Vps34/ultraviolet radiation resistance-associated gene (UVRAG) complex. *J. Biol. Chem.* 287:18359–18365. https://doi.org/10.1074/jbc.M112.367060

Makani, S.S., K.Y. Jen, and P.W. Finn. 2008. New costimulatory families: signaling lymphocytic activation molecule in adaptive allergic responses. *Curr. Mol. Med.* 8:359–364. https://doi.org/10.2174/156652408785161005

Mancuso, G., A. Midiri, C. Biondo, C. Beninati, S. Zummo, R. Galbo, F. Tomasello, M. Gambuzza, G. Macrì, A. Ruggeri, et al. 2007. Type I IFN signaling is crucial for host resistance against different species of pathogenic bacteria. *J. Immunol.* 178:3126–3133. https://doi.org/10.4049/jimmunol.178.5.3126

Mikhalap, S.V., L.M. Shlapatska, A.G. Berdova, C.L. Law, E.A. Clark, and S.P. Sidorenko. 1999. CDw150 associates with src-homology 2-containing inositol phosphatase and modulates CD95-mediated apoptosis. *J. Immunol.* 162:5719–5727.

Mogensen, T.H. 2009. Pathogen recognition and inflammatory signaling in innate immune defenses. *Clin. Microbiol. Rev.* 22:240–273. https://doi.org/10.1128/CMR.00046-08

Oshiumi, H., M. Sasai, K. Shida, T. Fujita, M. Matsumoto, and T. Seya. 2003. TIR-containing adapter molecule (TICAM)-2, a bridging adapter recruiting to toll-like receptor 4 TICAM-1 that induces interferon-beta. *J. Biol. Chem.* 278:49751–49762. https://doi.org/10.1074/jbc.M305820200

Pfaffl, M.W. 2001. A new mathematical model for relative quantification in real-time RT-PCR. *Nucleic Acids Res.* 29:e45. https://doi.org/10.1093/nar/29.9.e45

Poli-de-Figueiredo, L.F., A.G. Garrido, N. Nakagawa, and P. Sannomiya. 2008. Experimental models of sepsis and their clinical relevance. *Shock.* 30(Suppl 1):53–59. https://doi.org/10.1097/SHK.0b013e318181a343

Radtke, A.L., L.M. Delbridge, S. Balachandran, G.N. Barber, and M.X. O'Riordan. 2007. TBK1 protects vacuolar integrity during intracellular bacterial infection. *PLoS Pathog.* 3:e29. https://doi.org/10.1371/journal.ppat.0030029

Réthi, B., P. Gogolák, I. Szatmari, A. Veres, E. Erdôs, L. Nagy, E. Rajnavölgyi, C. Terhorst, and A. Lányi. 2006. SLAM/SLAM interactions inhibit CD40-induced production of inflammatory cytokines in monocyte-derived dendritic cells. *Blood.* 107:2821–2829. https://doi.org/10.1182/blood-2005-06-2265

Romanets-Korbut, O., A.M. Najakshin, M. Yurchenko, T.A. Malysheva, L. Kovalevska, L.M. Shlapatska, Y.A. Zozulya, A.V. Taranin, B. Horvat, and S.P. Sidorenko. 2015. Expression of CD150 in tumors of the central nervous system: identification of a novel isoform. *PLoS One.* 10:e0118302. https://doi.org/10.1371/journal.pone.0118302

Romero, X., D. Benítez, S. March, R. Vilella, M. Miralpeix, and P. Engel. 2004. Differential expression of SAP and EAT-2-binding leukocyte cell-surface molecules CD84, CD150 (SLAM), CD229 (Ly9) and CD244 (2B4). *Tissue Antigens.* 64:132–144. https://doi.org/10.1111/j.1399-0039.2004.00247.x

Sakaguchi, S., H. Negishi, M. Asagiri, C. Nakajima, T. Mizutani, A. Takaoka, K. Honda, and T. Taniguchi. 2003. Essential role of IRF-3 in lipopolysaccharide-induced interferon-beta gene expression and endotoxin shock. *Biochem. Biophys. Res. Commun.* 306:860–866. https://doi.org/10.1016/S0006-291X(03)01049-0

Sanjana, N.E., O. Shalem, and F. Zhang. 2014. Improved vectors and genome-wide libraries for CRISPR screening. *Nat. Methods.* 11:783–784. https://doi.org/10.1038/nmeth.3047

Schindelin, J., I. Arganda-Carreras, E. Frise, V. Kaynig, M. Longair, T. Pietzsch, S. Preibisch, C. Rueden, S. Saalfeld, B. Schmid, et al. 2012. Fiji: an open-source platform for biological-image analysis. *Nat. Methods.* 9:676–682. https://doi.org/10.1038/nmeth.2019

Schroder, K., K.M. Irvine, M.S. Taylor, N.J. Bokil, K.A. Le Cao, K.A. Masterman, L.I. Labzin, C.A. Semple, R. Kapetanovic, L. Fairbairn, et al. 2012. Conservation and divergence in Toll-like receptor 4-regulated gene expression in primary human versus mouse macrophages. *Proc. Natl. Acad. Sci. USA.* 109:E944–E953. https://doi.org/10.1073/pnas.1110156109

Shlapatska, L.M., S.V. Mikhalap, A.G. Berdova, O.M. Zelensky, T.J. Yun, K.E. Nichols, E.A. Clark, and S.P. Sidorenko. 2001. CD150 association with either the SH2-containing inositol phosphatase or the SH2-containing protein tyrosine phosphatase is regulated by the adaptor protein SH2D1A. *J. Immunol.* 166:5480–5487. https://doi.org/10.4049/jimmunol.166.9.5480

Sidorenko, S.P., and E.A. Clark. 1993. Characterization of a cell surface glycoprotein IPO-3, expressed on activated human B and T lymphocytes. *J. Immunol.* 151:4614–4624.

Theil, D., C. Farina, and E. Meinl. 2005. Differential expression of CD150 (SLAM) on monocytes and macrophages in chronic inflammatory contexts: abundant in Crohn's disease, but not in multiple sclerosis. *J. Clin. Pathol.* 58:110–111. https://doi.org/10.1136/jcp.2004.019323

Thurston, T.L., K.B. Boyle, M. Allen, B.J. Ravenhill, M. Karpiyevich, S. Bloor, A. Kaul, J. Noad, A. Foeglein, S.A. Matthews, et al. 2016. Recruitment of TBK1 to cytosol-invading Salmonella induces WIPI2-dependent antibacterial autophagy. *EMBO J.* 35:1779–1792. https://doi.org/10.15252/embj.201694491

Toshchakov, V., B.W. Jones, P.Y. Perera, K. Thomas, M.J. Cody, S. Zhang, B.R. Williams, J. Major, T.A. Hamilton, M.J. Fenton, and S.N. Vogel. 2002. TLR4, but not TLR2, mediates IFN-beta-induced STAT1alpha/beta-dependent gene expression in macrophages. *Nat. Immunol.* 3:392–398. https://doi.org/10.1038/ni774

Trinchieri, G. 2010. Type I interferon: friend or foe? *J. Exp. Med.* 207:2053–2063. https://doi.org/10.1084/jem.20101664

Troutman, T.D., W. Hu, S. Fulenchek, T. Yamazaki, T. Kurosaki, J.F. Bazan, and C. Pasare. 2012. Role for B-cell adapter for PI3K (BCAP) as a signaling adapter linking Toll-like receptors (TLRs) to serine/threonine kinases PI3K/Akt. *Proc. Natl. Acad. Sci. USA.* 109:273–278. https://doi.org/10.1073/pnas.1118579109

van Driel, B., G. Liao, X. Romero, M.S. O'Keeffe, G. Wang, W.A. Faubion, S.B. Berger, E.M. Magelky, M. Manocha, V. Azcutia, et al. 2012. Signaling lymphocyte activation molecule regulates development of colitis in mice. *Gastroenterol.* 143:1544–1554.

van Driel, B.J., G. Liao, P. Engel, and C. Terhorst. 2016. Responses to Microbial Challenges by SLAMF Receptors. *Front. Immunol.* 7:4. https://doi.org/10.3389/fimmu.2016.00004

Vaure, C., and Y. Liu. 2014. A comparative review of toll-like receptor 4 expression and functionality in different animal species. *Front. Immunol.* 5:316. https://doi.org/10.3389/fimmu.2014.00316

Wang, N., A. Satoskar, W. Faubion, D. Howie, S. Okamoto, S. Feske, C. Gullo, K. Clarke, M.R. Sosa, A.H. Sharpe, and C. Terhorst. 2004. The cell surface receptor SLAM controls T cell and macrophage functions. *J. Exp. Med.* 199:1255–1264. https://doi.org/10.1084/jem.20031835

West, A.P., I.E. Brodsky, C. Rahner, D.K. Woo, H. Erdjument-Bromage, P. Tempst, M.C. Walsh, Y. Choi, G.S. Shadel, and S. Ghosh. 2011. TLR signalling augments macrophage bactericidal activity through mitochondrial ROS. *Nature.* 472:476–480. https://doi.org/10.1038/nature09973

Yamamoto, M., S. Sato, H. Hemmi, S. Uematsu, K. Hoshino, T. Kaisho, O. Takeuchi, K. Takeda, and S. Akira. 2003. TRAM is specifically involved in the Toll-like receptor 4-mediated MyD88-independent signaling pathway. *Nat. Immunol.* 4:1144–1150. https://doi.org/10.1038/ni986

Yamashiro, D.J., B. Tycko, S.R. Fluss, and F.R. Maxfield. 1984. Segregation of transferrin to a mildly acidic (pH 6.5) para-Golgi compartment in the recycling pathway. *Cell.* 37:789–800. https://doi.org/10.1016/0092-8674(84)90414-8